Check for updates

Margin processes sculpting a land-detached canyon-channel system: the Gollum Channel System in the Porcupine Seabight

L. Verweirder[1]*, D. Van Rooij[1] and A. Georgiopoulou[2]

[1]Department of Geology, Ghent University, Ghent, Belgium, [2]Ternan Energy, Chichester, United Kingdom
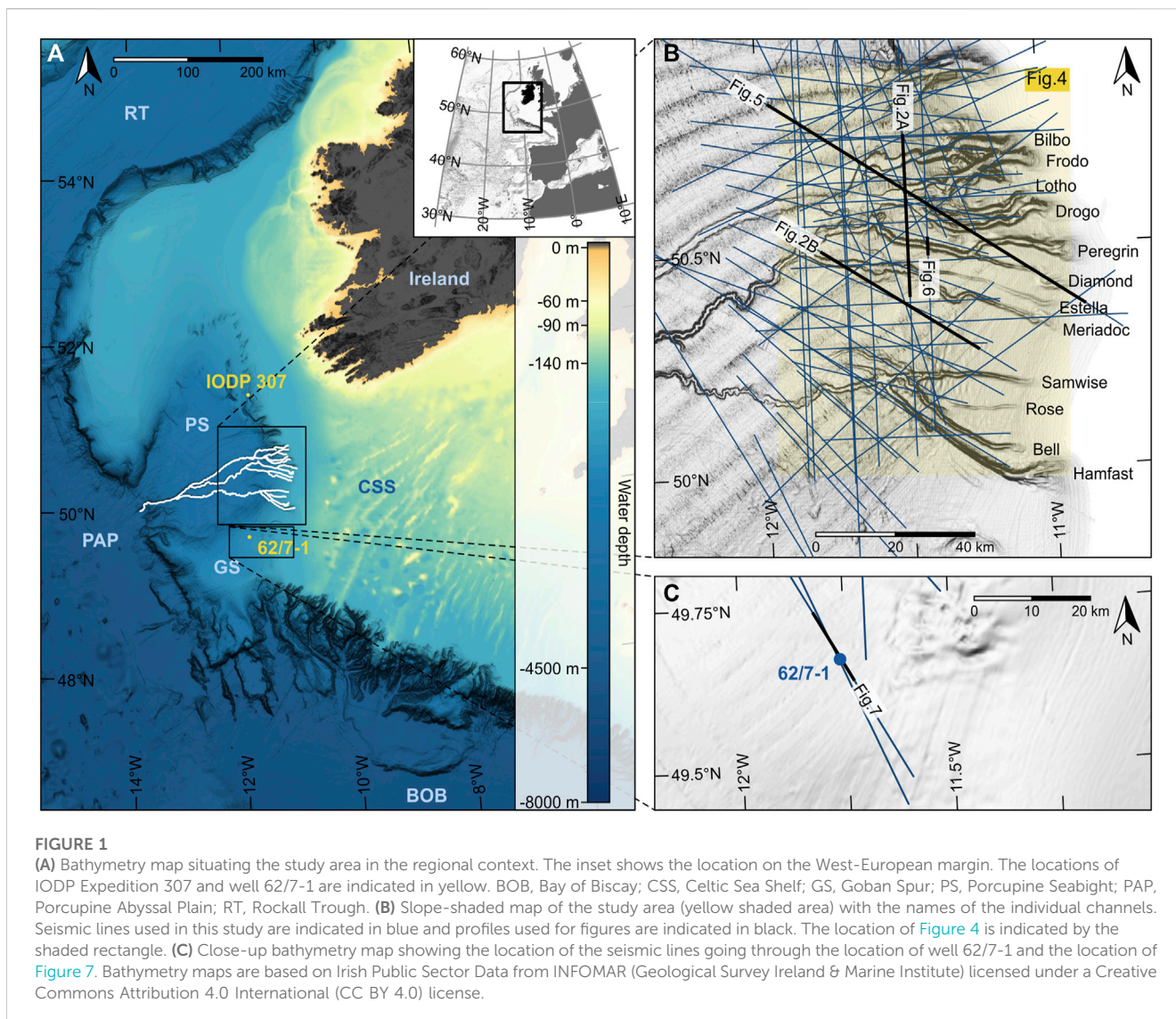
The land-detached Gollum Channel System (GCS) is one of very few large-scale canyon-channel systems on the Northwest European margin and thought to be of high importance in both along-slope and downslope sediment transport processes in the Porcupine Seabight basin. It is, however, unknown when this system was formed and how active it has been throughout its evolution, making it difficult to assess its regional impact. Here, using well data integrated with airgun seismic reflection data, a seismic stratigraphy (Cretaceous to present) is built for the GCS for the first time. We find that, contrary to what was thought before, the GCS was formed before Quaternary glaciations occupied the continental shelf and its origin is tentatively associated to a phase of Northeast Atlantic margin tilting in the early Pliocene. Each of the channels that make up the GCS was initiated by incision from erosive downslope gravity flows originating on the Celtic Sea Shelf. Gravity flows from Quaternary glacial processes reused the channels and mostly bypassed the upper slope or contributed to the channel fill, though some flows were capable of erosion of existing channel flanks and incision of several smaller channels. Additionally, we show that this margin was incised by erosive gravity flows on several occasions through time and that these incisions seem to follow preferential pathways. Interaction with along-slope bottom currents from the start of the Quaternary onwards was crucial to distribute sediments and nutrients to sediment drifts and cold-water coral mounds further north (downstream) along the Irish margin.

1 Introduction

Large-scale submarine canyon-channel systems, present on continental shelves and slopes across the world (Harris and Whiteway, 2011), are preferential pathways for the transport of sediment, organic matter and pollutants into the adjacent basins. They are often associated with high terrestrial sediment supply from, e.g., fluvial systems (Khripounoff et al., 2012; Babonneau et al., 2013; Puig et al., 2017) or ice sheets (Zaragosi et al., 2006; Rise et al., 2013). Additionally, several processes, such as trawling (Martín et al., 2014; Daly et al., 2018), dense water cascading (Canals et al., 2006; Puig et al., 2013), earthquakes (Mountjoy et al., 2014), tidal currents (Mulder et al., 2012; Amaro et al., 2016), and storm waves (Puig et al., 2004) are capable of resuspending shelf and slope sediments and transporting them down (or up; Amaro et al., 2016) canyon axes. This ensures the role of canyon-channel systems in sediment transport even when they are not connected to terrestrial sources. Furthermore,

FIGURE 1
(A) Bathymetry map situating the study area in the regional context. The inset shows the location on the West-European margin. The locations of IODP Expedition 307 and well 62/7-1 are indicated in yellow. BOB, Bay of Biscay; CSS, Celtic Sea Shelf; GS, Goban Spur; PS, Porcupine Seabight; PAP, Porcupine Abyssal Plain; RT, Rockall Trough. **(B)** Slope-shaded map of the study area (yellow shaded area) with the names of the individual channels. Seismic lines used in this study are indicated in blue and profiles used for figures are indicated in black. The location of Figure 4 is indicated by the shaded rectangle. **(C)** Close-up bathymetry map showing the location of the seismic lines going through the location of well 62/7-1 and the location of Figure 7. Bathymetry maps are based on Irish Public Sector Data from INFOMAR (Geological Survey Ireland & Marine Institute) licensed under a Creative Commons Attribution 4.0 International (CC BY 4.0) license.

these systems can have a considerable influence on local and regional hydrography (Voigt et al., 2013; Waterhouse et al., 2017; Verweirder et al., 2021). Considering the significant role large-scale canyon-channel systems have in conducting and redistributing sediment, it is important to understand the processes that shape them.

The Gollum Channel System (GCS) is the only large-scale channel system on the Northwest European margin (Weaver et al., 2000) and stretches over c. 200 km connecting the Celtic Sea Shelf to the Porcupine Abyssal Plain (Figure 1). The system was named by Kenyon et al. (1978) and the names of the individual channels were given by Van Rooij (2004) (Figure 1B). The GCS presently has no apparent connection to any terrestrial sediment sources and is not thought to be active with downslope gravity flows (Akhmetzhanov et al., 2003; Wheeler et al., 2003). It did have a large influence on regional processes in the past as it is thought to have supplied sediments to the cold-water coral mounds and contourite drifts in the Belgica Mound Province (BMP; Van Rooij et al., 2007b; Van Rooij et al., 2009; Verweirder et al., 2021). It is, however, unknown when the system was formed and thus when its regional

influence started, as well as which processes were involved in creating it. This is in stark contrast to the Celtic and Armorican systems in the Bay of Biscay, for which the history of activity has been thoroughly investigated (Mulder et al., 2012; Amaro et al., 2016; Hall et al., 2017; Aslam et al., 2018; Heijnen et al., 2022) and linked to the activity of the Fleuve Manche paleoriver (Bourillet et al., 2003; Zaragosi et al., 2006; Toucanne et al., 2008; 2009; 2012).

A causal relationship between erosive downslope currents associated with the start of glacial-interglacial cycles in the North Atlantic and the formation of the GCS has been suggested from Neogene-Quaternary seismic stratigraphy (Verweirder et al., 2021). However, the dataset used by those authors is not sufficient for this investigation, as the GCS channel bases are situated below the penetration depth of their seismic data. Therefore, the origin of the GCS and the potential link with Quaternary glacial-interglacial cycles needs further examination that is based on seismic data also covering the deeper subsurface. Previous stratigraphic studies in the Porcupine Seabight have focused on the Neogene and Quaternary stratigraphy in the area of the BMP (Van Rooij et al., 2003; Van Rooij et al., 2009; Thierens et al., 2012), on the very general Cenozoic

stratigraphy of the basin (McDonnell and Shannon, 2001; Stoker et al., 2005a), and briefly on the morphology of the GCS channel heads (Wheeler et al., 2003), but never comprehensively on the stratigraphy of the GCS channels.

The aim of this study is to investigate which processes were involved in the formation of the GCS and to assess the spatiotemporal evolution of the system. To this end, a seismic stratigraphic framework was built from the channel heads on the upper slope down to the foot of the slope and from the acoustic basement to the present-day seafloor.

2 Geological setting

The GCS is situated in the southern part of the Porcupine Seabight, a pear-shaped oceanic basin that forms an embayment on the northeast Atlantic margin (Figure 1A). The Porcupine Seabight is the surface expression of the Porcupine Basin, a failed rift basin that formed from the Permian onwards (Shannon, 1991). It owes its north-south elongation to a major Late Jurassic rifting episode with east-west extension associated with North Atlantic seafloor spreading (Shannon, 1991; Naylor and Shannon, 2005; Shannon et al., 2007). The basin experienced thermal subsidence from the Early Cretaceous to the Holocene (Shannon, 1991). Open marine conditions were established for the first time in the Late Cretaceous (McCann et al., 1995; McDonnell and Shannon, 2001), and, after a period of regression in the late Paleocene–late Eocene (Moore and Shannon, 1992), again and finally in the latest Eocene–earliest Oligocene (McDonnell and Shannon, 2001; Stoker et al., 2005b).

A major uppermost Eocene erosional unconformity (regionally identified on seismic data as a high-amplitude reflection called reflector C30) marks the onset of deep-water current circulation in the basin and the change from downslope- to along-slope-dominant sediment transport characterized by drift deposition (Stoker et al., 2001; Stoker et al., 2005b; Shannon et al., 2005). The circulation pattern changed in the early to middle Miocene from Tethyan-influenced bottom current activity to Nordic seas-influenced bottom current activity (Stoker et al., 2005b), resulting in an uppermost lower Miocene regional unconformity (regional seismic reflector C20; McDonnell and Shannon, 2001). In the Rockall Trough, the high amplitude of the C20 reflection may be further enhanced by the presence of a diagenetically altered ash layer (Stoker et al., 2001). Another period of extensive contourite drift development in the middle to late Miocene (McDonnell and Shannon, 2001; Shannon et al., 2005) was ended by an episode of regional submarine erosion (regional seismic reflector C10 characterized by a continuous reflection of high amplitude) likely from increased North Atlantic Deep Water input from the Nordic seas along with basin margin tilting in the early Pliocene (Stoker et al., 2001; 2005a; 2005b). The youngest stratigraphic interval is characterized by the presence of coral mounds and contourite drifts, and the upper Quaternary sedimentation is influenced by glacial activity (Tudhope and Scoffin, 1995; Van Rooij et al., 2007b). The Porcupine Basin contains up to 6 km of Mesozoic sediments and the Cenozoic fill is up to 4 km thick (Moore and Shannon, 1992; McDonnell and Shannon, 2001).

Over the eastern upper slope of the basin, previous studies have recognized a discontinuity that was attributed an early middle Miocene age (seismic reflector RD2 of Van Rooij et al. (2003)) (Louwye et al., 2008) and a discontinuity representing a hiatus between upper Miocene and upper Pliocene sediments (seismic reflector RD1 of Van Rooij et al. (2003)) (Kano et al., 2007; Louwye et al., 2008; Van Rooij et al., 2009). They have been proposed as equivalents to the regional latest early Miocene (C20) and early Pliocene (C10) unconformities, respectively (Van Rooij et al., 2003), but have never been tied on any seismic line. In the specific setting of the eastern slope of the Porcupine Seabight, the origin of the RD1 discontinuity has been pinpointed in more detail than the C10 unconformity. The RD1 discontinuity is the result of the combined action of both along-slope and downslope currents associated with, respectively, the influence of the Mediterranean Outflow Water on the oceanographic regime in the Seabight, and the onset of glacial-interglacial cycles in the North Atlantic (Van Rooij et al., 2003). The main sediment source for the Quaternary downslope gravity currents is the Celtic Sea Shelf, with principal supply during lowered sea levels of glacial periods (Akhmetzhanov et al., 2003). The RD1 seismic reflector is very obvious from its erosional characteristics and the distinct differences between the units above and below in the BMP, but is known to become harder to trace to the south, towards the study area (Verweirder et al., 2021).

3 Materials and methods

To build the seismic stratigraphy needed for this study, well data were integrated with seismic reflection data, which were then analyzed considering the seismic stratigraphy that was established in other parts of the Porcupine Seabight by McDonnell and Shannon (2001), Van Rooij et al. (2003), and Van Rooij et al. (2009). These studies are also the basis for the nomenclature of the seismic units and their bounding surfaces used here (Figure 2): C30 from McDonnell and Shannon (2001), and RD2 and RD1 from Van Rooij et al. (2003) and Van Rooij et al. (2007a).

The four multichannel seismic reflection datasets used in this work (Nopec Geoventures 1997, Geco-Prakla 1997, Fugro-Geoteam 1997 and Spectrum 1997) were provided by the Irish Department of the Environment, Climate and Communications. All four were recorded in 1997 with airgun sources. They were processed prior to receiving them, with processing steps including dip moveout, stacking, deconvolution, as well as several filters depending on the dataset. A brief overview of the processing flow used for each dataset can be found in Supplementary Table S1 and some additional details are available on the website of the Irish Department of Communications, Energy and Natural Resources (Department of Communications, Energy and Natural Resources, 2010). The datasets are used here without any additional processing. The dominant frequency in the seismic data is 5–70 Hz, and their vertical resolution decreases from c. 10 m in the shallow subsurface to c. 20–30 m near the acoustic basement. The profiles were loaded into S&P Global Kingdom software for analysis of the reflectors and integration with well data. Within the Kingdom software, a mistie analysis including time shifts, phase shifts and amplitude scaling was performed to allow good correlation between the four datasets.

Key horizons were first identified in the Kingdom software and then gridded to acquire paleotopography maps using the Surfer

package from Golden Software. Kriging was found to be the gridding method that produced the most realistic maps. The grid spacing was set to 100 m. Thickness maps of specific stratigraphic sections were also created in Surfer.

The drainage networks used to compare the present-day channel network to depressions in paleotopographical surfaces were generated using the "Generate Watershed" analysis tool in Global Mapper software, which is based on the eight-direction pour point algorithm from Jenson and Domingue (1988) to determine the flow direction at each point of the analyzed grid. The horizontal resolution of the watershed was set equal to the resolution of the analyzed grid (100 m). As the focus is on the large-scale drainage pattern of the area, the stream cell threshold was set to 500 and the smallest secondary thalweg sections were removed. Minimal smoothing of calculated thalwegs was done manually. To calculate the amount of overlap between the locations of the present-day channel thalwegs and depressions in the paleotopography, buffers were first created around the main thalwegs of the paleowatershed. The widths of the buffers correspond to the widths of the paleodepressions and were measured on the appropriate reflector in the seismic data. Then, the length of the present-day thalwegs intersecting the paleowatershed buffers was divided by the total length of the present-day thalwegs in the study area. Thus, a percentage value for the amount of overlap between the locations of the present-day watershed and the paleowatershed was obtained.

Age control of the seismic data was partly achieved through time-depth conversion of the stratigraphy at well 62/7-1. Well data were provided by the Irish Department of the Environment, Climate and Communications and included descriptions of lithological and paleontological samples, log data, interval velocity data, and the well completion report. Well 62/7-1 is located on Goban Spur (Figure 1) at 993 m water depth and reaches a total depth of 3,669 m below the seafloor, targeting potential Bathonian and Sinemurian reservoirs. The time-depth conversion of the stratigraphy at well 62/7-1 was performed using data from two airgun vertical seismic profiles covering complementary depth intervals. In these surveys, the travel time between source and receiver is measured and the distance between them is used to calculate average velocities and interval velocities at the location of the well. The results of both surveys were combined and are shown in Supplementary Figure S1. Since this well is located >100 km from the most distant (northern) part of the study area, time-depth conversion was only performed at the location of the well. All depths related to well 62/7-1 are reported with respect to the seabed. The well stratigraphy is based on downhole logging data, and paleontology and lithology obtained from cuttings and side wall cores described in the well reports. In this well, the shallowest sample was taken at a depth of 615 m, so the well data could only be tied to the deepest sections of the seismic data.

The chronostratigraphy of the shallower seismic data was based on the previously established general Cenozoic seismic stratigraphy of the Porcupine Seabight (McDonnell and Shannon, 2001; Shannon et al., 2005) and the Neogene and Quaternary seismic stratigraphy of the BMP (Van Rooij et al., 2003; Van Rooij et al., 2009). These stratigraphies were in turn based on well data from sixteen exploration and appraisal wells (McDonnell and Shannon, 2001), and data from the IODP 307 boreholes (Van Rooij et al., 2009).

Tying the seismic data used here to the previously established stratigraphy was possible due to distinct similarities in seismic expression and a direct seismic connection between the study area and the BMP.

4 Results

4.1 Seismic reflection data

Generally, the sedimentary fill of the Porcupine Basin displays a catenary geometry: horizons are near-horizontal in the center of the basin and dip towards the basin center (with a greater dip further away from the center) on the edges (Figure 2B). Five seismic units (U5—U1; from old to young) bounded by six reflectors (basement, NTC, C30, RD2, RD1, seafloor; from old to young) have been identified from the acoustic basement to the seafloor (Figure 2). A seventh reflector (ECP) is considered as an internal reflector in seismic unit U2, but as it is seen as a key reflector in the evolution of the GCS, it is here described separately.

4.1.1 Key seismic reflectors

The basement reflector is the deepest high-amplitude reflection that is mostly continuous and represents the boundary between the discontinuous to chaotic facies of the acoustic basement and the more continuous facies of the overlying seismic units (Figure 2). It is a surface with a very irregular topography and often has an erosional character.

The near top Cretaceous (NTC) reflector is characterized by a moderate-to high-amplitude reflection and is generally continuous in the basin (Figure 2). A paleo-shelf break is inferred from a change in slope gradient in the seismic data at c. 2–2.2 s TWT (Figure 3A). The outermost part of the paleo-shelf has an irregular topography but is generally quasi horizontal to slightly basinward-dipping (2°–3°). The steeply dipping (10°–15°) paleo-slope section is smooth to irregular and generally becomes smoother towards the foot of the slope and into the basin, where it displays large-scale undulations of small amplitude and irregular wavelength (Figure 2). The NTC reflector is conformable to over- and underlying reflectors in the basin, but erosional on the paleo-slope and near the paleo-shelf break. On the paleo-shelf, it often coincides with the basement reflector. In the absence of obvious seismic terminations the relation to the underlying package is difficult to determine.

The C30 reflector has a wavy to irregular topography and a high-amplitude reflection (Figure 3B). It is offset by numerous faults and the identification of this reflector becomes more uncertain towards the south and east. Within the study area, the C30 surface displays six NE-SW to SE-NW oriented channels. Data in the northwesternmost part of the study area suggest more channels are present to the north (Figure 3B). The channels observed here are c. 3–13 km wide and c. 100–500 m deep. At the channel bases and edges, the otherwise conformable C30 reflector truncates the reflectors of the seismic unit below (Figure 2C). Near the eastern edge of the study area, the C30 reflector is part of a package of reflectors that onlaps the NTC reflector.

The RD2 reflector is erosional to conformable, and, like the C30 reflector, it is offset by numerous faults (Figure 2). It has a
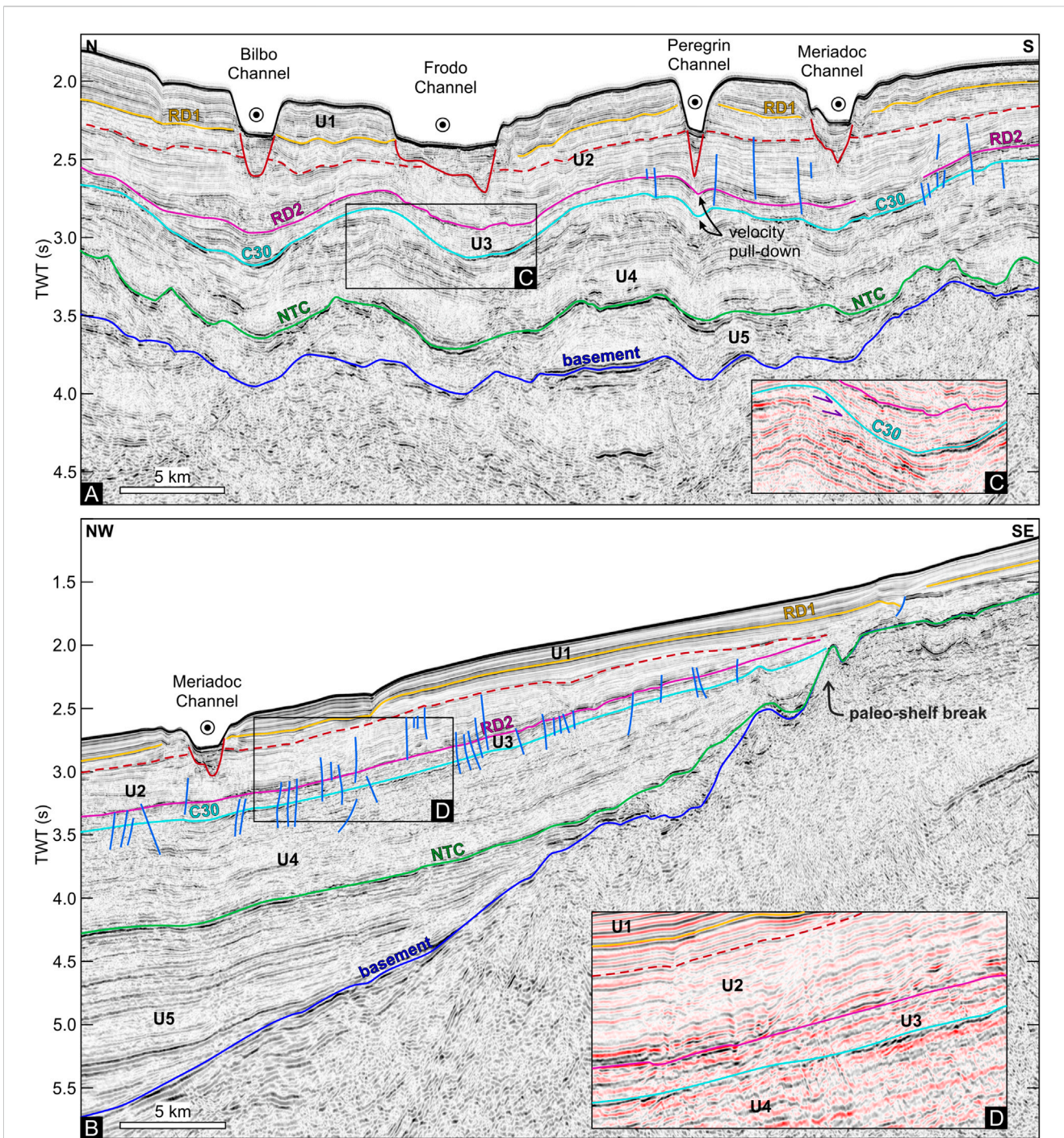
FIGURE 2
(A,B) Interpreted airgun seismic reflection profile showing the five units (U1–U5) and their boundaries (seafloor, RD1, RD2, C30, NTC, basement) that make up the general stratigraphy of the study area. The bases of the present-day GCS are indicated in red. Faults are marked in blue. The ECP reflector is indicated as a red dashed line. The locations are shown in Figure 1B. **(C)** Closeup of the seismic profile in **(A)** showing the erosion (purple arrows) underneath the C30 reflector at the top of unit U4. **(D)** Closeup of the seismic profile in **(B)** highlighting the difference in seismic facies between units U3 and U2.

large-scale undulating appearance in N-S profiles, especially towards the upper slope. The RD2 undulation pattern mimics that of the C30 reflector: RD2 lows, though they are less pronounced than the C30 paleochannels, are situated over the C30 paleochannels (Figure 3C). The RD2 reflector is only moderately continuous, which makes it difficult to trace

towards the south and the east, where it also loses its erosional characteristics. A change in seismic facies, generally from more faulted just below the reflector to slightly more distinct and continuous stratification, sometimes with higher amplitude, just above the reflector, may then help in identifying it (Figure 2D). Though the RD2 reflector can be traced towards the present-day
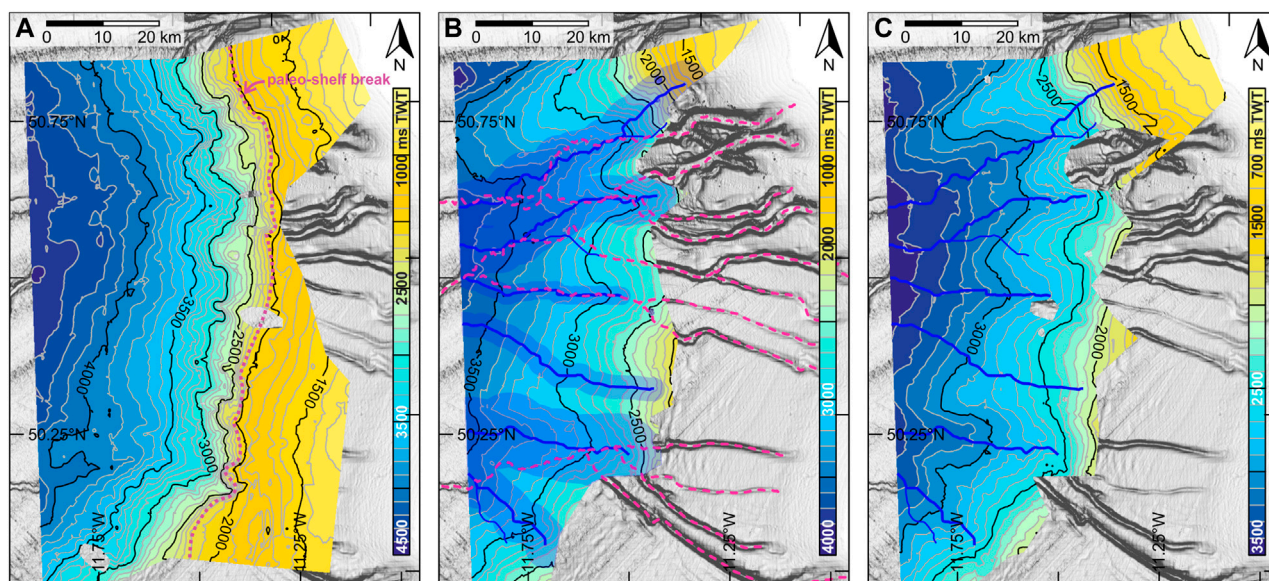
FIGURE 3
Paleotopography maps of the **(A)** NTC, **(B)** C30, and **(C)** RD2 surfaces expressed in ms TWT from present-day sea level plotted over a slope-shaded bathymetry map of the present-day seabed. **(A)** The interpreted paleo-shelf break is indicated by a pink dotted line. **(B)** The watershed of the C30 paleochannels is indicated in blue solid lines and the buffers of the main paleochannels are shaded blue. The thalwegs of the present-day GCS are indicated in pink dashed lines. **(C)** The watershed of the C30 paleochannels [identical to **(B)**] is indicated in blue solid lines. Note that the color scales of the three maps differ.

shelf edge in the northernmost part of the study area, it either onlaps one of the underlying units or is eroded by overlying reflectors at the upper slope in the rest of the study area.

The early channel presence (ECP) reflector is characterized by a moderate-amplitude reflection. It is conformable to (small-scale) erosional and has an overall smooth topography without any significant features. It is only present in the northern and central parts of the study area, and is eroded by overlying reflectors in the upslope and southern parts of the study area.

The RD1 reflector is mostly continuous and conformable with the under- and overlying reflectors in the GCS interfluve areas. It can be truncated and/or truncating at the GCS channel edges. It has an overall smooth topography without the large wavy structures that the RD2 and C30 reflectors have. The main feature in the RD1 paleotopography are the gaps caused by the incisions at the base of the present-day GCS.

4.1.2 Seismic stratigraphy

Unit U5 is the lowermost seismic unit that can be distinguished above the acoustic basement (Figure 2). It consists of (sub)parallel reflections that onlap the acoustic basement, filling in the basin. The reflections are mostly continuous, have moderate to high amplitudes, and are sub-horizontal though in some places slightly wavy towards the center of the basin (Figure 2). The NTC reflector bounding the top of the unit truncates U5 reflectors near the basin margin but is conformable in the basin center. The unit pinches out against the basement at the basin margins and is not present east of the inferred NTC paleo-shelf break (Figure 2B). The thickness of unit U5 increases from the basin margins to the basin center to 2 s TWT (Figure 4A).

Unit U4 is bound by the NTC reflector at the bottom and the C30 reflector at the top. It consists of (sub)parallel to slightly mounded reflections of low to moderate amplitude that are mostly continuous, except for some places where localized internal erosion is visible within the unit (Figure 5C). Additionally, the channels of the C30 reflector cut down into unit U4 and remove the upper 200–500 ms TWT of the unit. The thickness of unit U4 increases from 0 s TWT on the upper slope, where it onlaps against the steep slope created by the NTC reflector, to 950 ms TWT in the basin, where it fills up the topography of the NTC reflector (Figure 4B). Thicker packages in this unit correspond to the interfluve areas of the C30 paleochannels.

Unit U3 is bound by the C30 (bottom) and RD2 (top) reflectors. It contains reflections that are generally lower in amplitude compared to unit U4 and are disrupted by a multitude of faults (Figure 5A). Reflectors are mostly subparallel to very slightly mounded though the faulting can make them look very discontinuous and almost chaotic (Figure 2B). The U3 reflectors infill the inferred C30 channels and drape the C30 reflector where it created topographic highs (Figures 2, 5). Like unit U4, unit U3 pinches out towards the eastern edge of the basin. The thickness of U3 varies mostly between 0 and 250 ms TWT, except in the northwesternmost part of the study area, where a thick (500 ms TWT) package is present (Figure 4C). This thicker package is elongated in a NE-SW direction and its location and geometry correspond to a C30 paleochannel just northwest of the study area. In general, unit U3 is thicker where it fills the C30 paleochannels and thinner on the topographic highs. In the
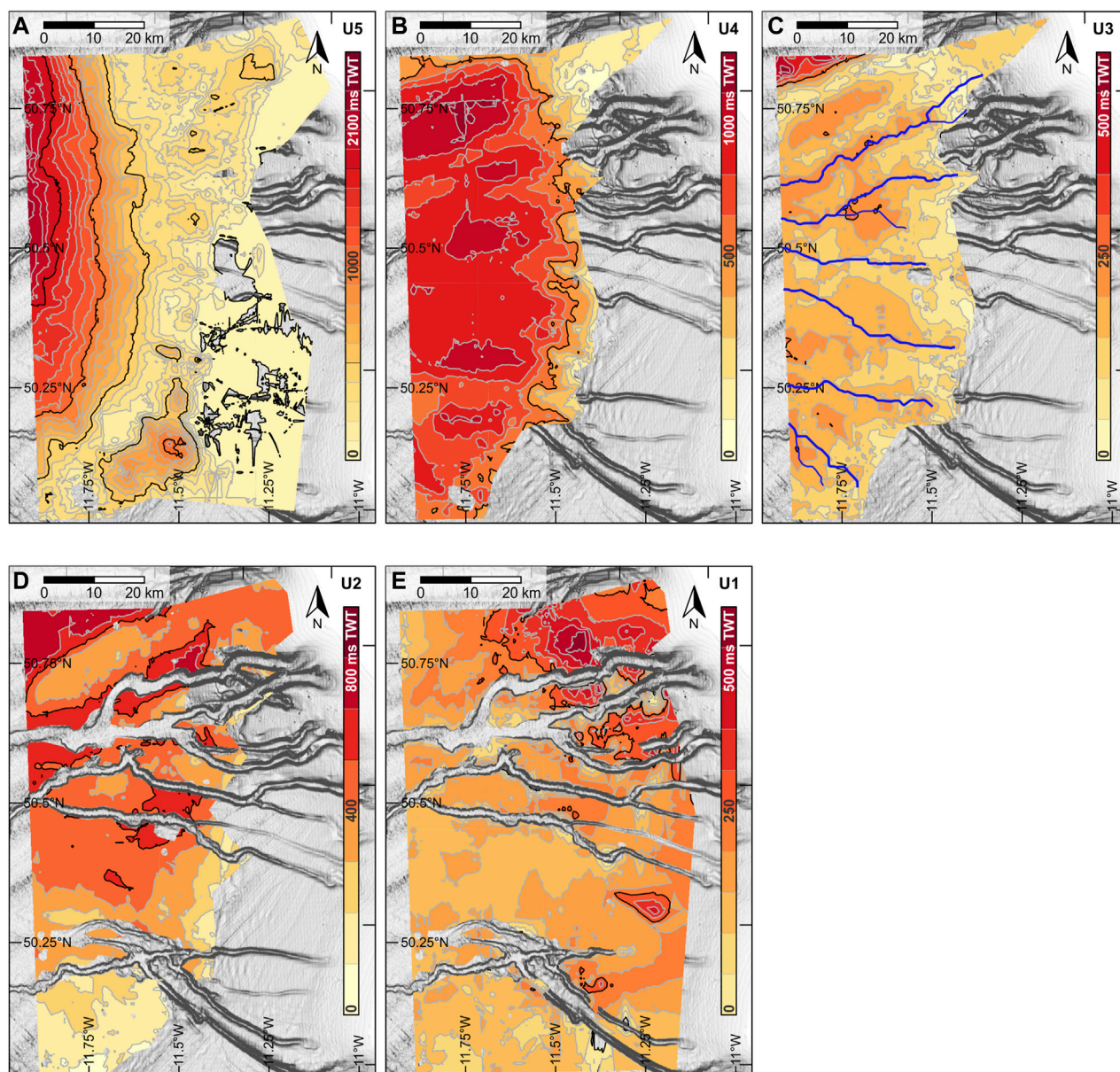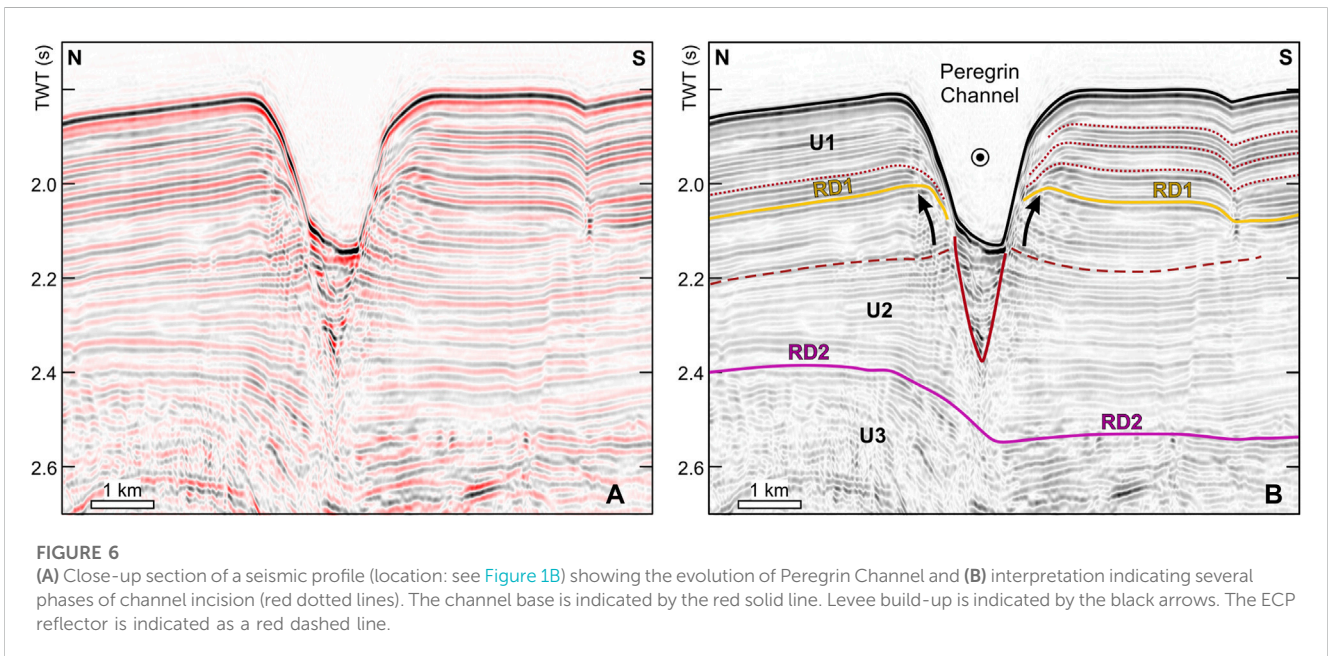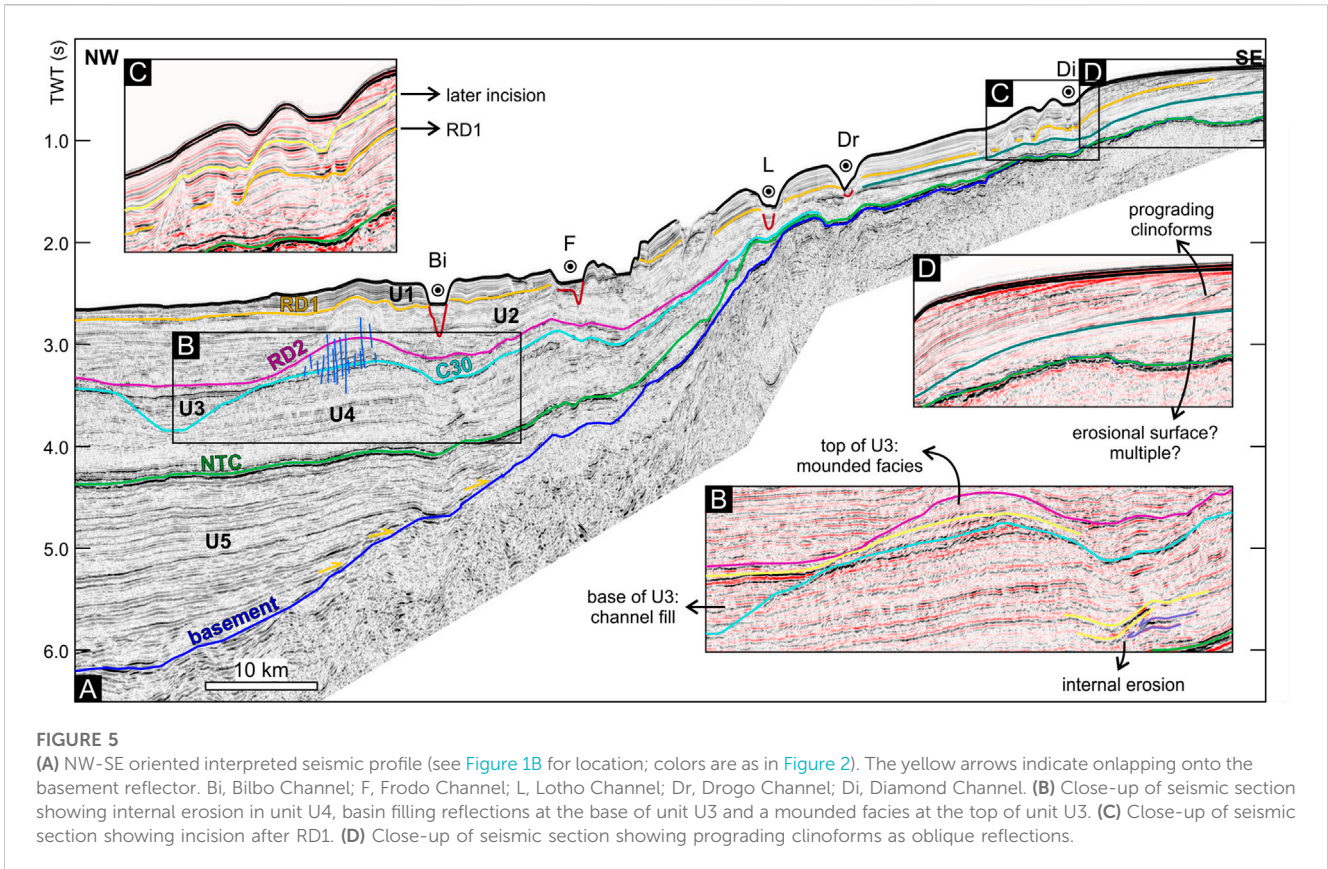
FIGURE 4
Isopach maps (plotted on top of present-day slope-shaded bathymetry maps) of **(A)** unit U5 between the acoustic basement and NTC reflectors, **(B)** unit U4 between reflectors NTC and C30, **(C)** unit U3 between reflectors C30 and RD2, where the thalwegs of the C30 surface are indicated in blue solid lines, **(D)** unit U2 between reflectors RD2 and RD1, and **(E)** unit U1 between reflector RD1 and the seafloor. The isopachs are calculated only where both bounding reflectors are present. This creates discontinuities in the maps, especially underneath the present-day GCS where the incisions at the channel bases cut through units U2 **(D)** and U1 **(E)**. See Figure 1B for the location of the study area. Note that the color scale differs in each panel.

northernmost part of the study area, however, the lower part of unit U3 consists of horizontal reflectors that fill one of the C30 paleochannels while the top of the unit has a mounded geometry and is preferentially deposited on the interfluve (Figure 5C). The mounded geometry of the upper part of U3 here is also visible as a thicker package in the isopach map (Figure 4C).

The base of unit U2 is the RD2 reflector, while at the top it is bound by the RD1 reflector. Where present, the ECP reflector is contained in this unit. The reflections within unit U2 have a low to

moderate amplitude similar to unit U3 below. The bases of the present-day GCS channels locally remove 50–>400 ms TWT at the top of the unit. Although unit U2 is dissected by numerous faults, the reflections are generally laterally traceable over long distances. They dip towards the center of the basin, and onlap or drape the RD2 reflector. In proximity (1–2 km) to the channel bases of the present-day GCS, U2 reflections may be divergent (Figure 6). The thickness of unit U2 generally decreases towards the upper slope and to the south, varying between 0 and 750 ms TWT (Figure 4D). When comparing the thickness distribution of unit U2 with the

FIGURE 5
(A) NW-SE oriented interpreted seismic profile (see Figure 1B for location; colors are as in Figure 2). The yellow arrows indicate onlapping onto the basement reflector. Bi, Bilbo Channel; F, Frodo Channel; L, Lotho Channel; Dr, Drogo Channel; Di, Diamond Channel. **(B)** Close-up of seismic section showing internal erosion in unit U4, basin filling reflections at the base of unit U3 and a mounded facies at the top of unit U3. **(C)** Close-up of seismic section showing incision after RD1. **(D)** Close-up of seismic section showing prograding clinoforms as oblique reflections.

FIGURE 6
(A) Close-up section of a seismic profile (location: see Figure 1B) showing the evolution of Peregrin Channel and **(B)** interpretation indicating several phases of channel incision (red dotted lines). The channel base is indicated by the red solid line. Levee build-up is indicated by the black arrows. The ECP reflector is indicated as a red dashed line.

RD2 paleotopography, it is apparent that the unit heals the RD2 paleotopography being thicker in the lows and thinner on RD2 paleo-highs (compare Figure 3C and Figure 4D).

Unit U1 is the uppermost seismic unit between the RD1 reflector and the seafloor. It is characterized by channels cutting through the unit, sometimes all the way to and through the base. The moderate-

to high-amplitude reflections of unit U1 are well-stratified, parallel, dipping towards the basin center, conformable and continuous, except at the channel edges of the present-day GCS, where they are generally truncated and locally divergent. Wavy reflector configurations can be found in proximity to some of the channels. Unit U1 is thickest on the upper slope present-day interfluves, especially surrounding the two northernmost channels (Figure 4E). The thickness of the unit generally decreases to the south and there is some pinching out of reflectors towards the basin center, which is reflected in a thickness decrease downslope from 500 ms TWT to 100 ms TWT (Figure 4E).

4.1.3 Comparison of paleo- and present-day watersheds

Calculated watersheds show that the thalwegs of the present-day channel system are often situated close to or on top of the C30 paleochannels. Where the C30 reflector is present (colored area in Figure 3B), 85% of the present-day thalwegs intersect with a C30 paleochannel. When also considering the upslope sections of the present-day channels where the C30 reflector is not present due to erosion or onlapping, 34% of the channel sections intersect with a C30 paleochannel.

4.2 Well 62/7-1 and ties to seismic data

As lithological samples and all logs except for the gamma ray log were retrieved from below 560 m depth below the seafloor, the well data can only be used to link the deeper parts of the seismic stratigraphy (seismic unit U5 and part of seismic unit U4) to the Middle Jurassic to early Eocene sections of the well stratigraphy.

At the location of well 62/7-1 (Figure 1), the acoustic basement is not easily identified but is likely situated at 2,330 m depth, at the top of a section of calcareous shales of early Bajocian age. It corresponds to a sharp upwards decrease in gamma ray, neutron porosity and sonic velocity (Figure 7).

Seismic unit U5 consists of (calcareous) siltstones and claystones at the bottom, followed by a sandstone section with a c. 220 m-thick section of volcanic rocks on top. At 2,070–2,060 m
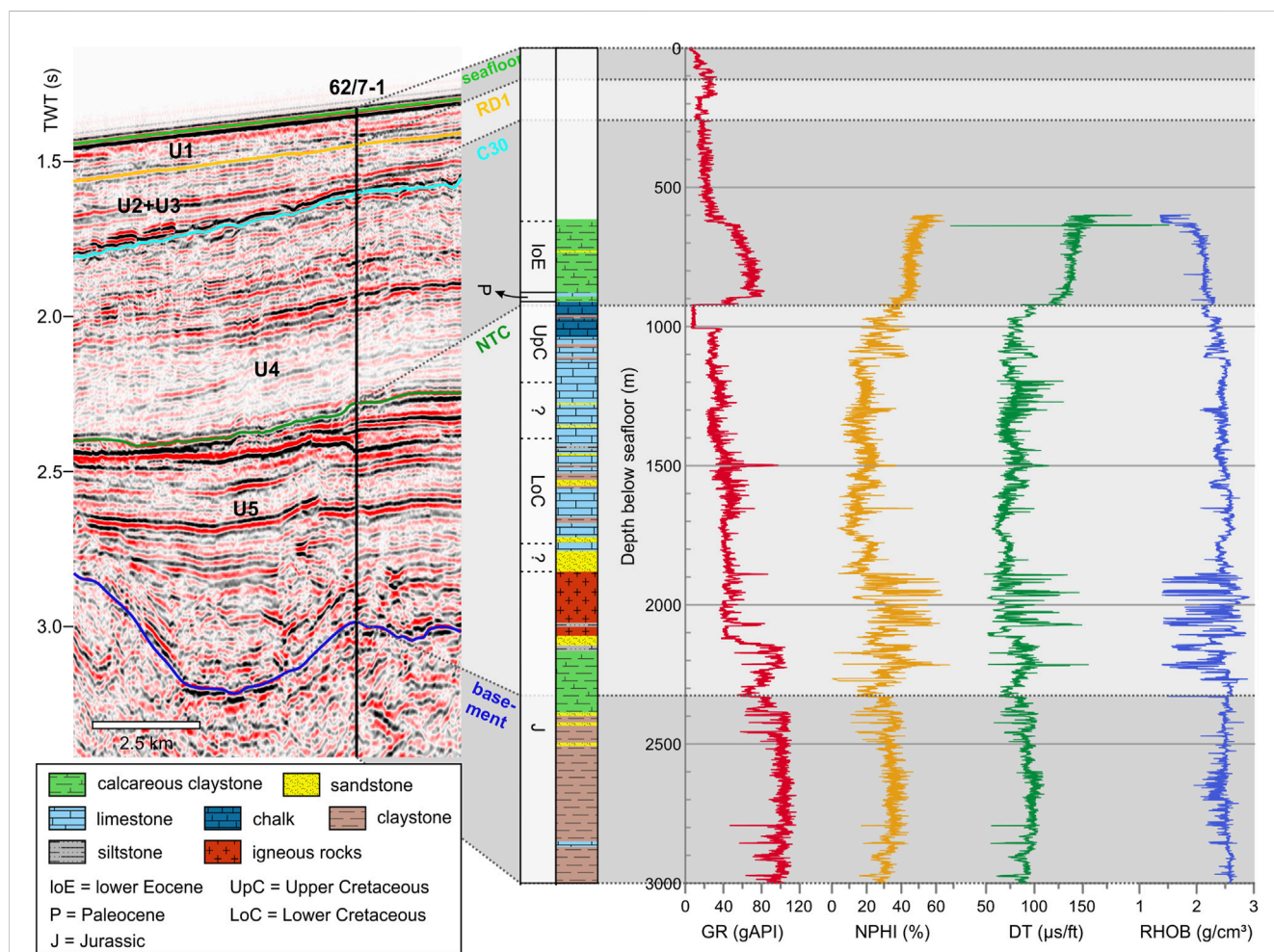
FIGURE 7
A section of a seismic line crossing well 62/7-1 (see Figure 1 for location) illustrating the correlation between well (from left to right: lithology, gamma ray log (GR), neutron density log (NPHI), sonic velocity log (DT) and density log (RHOB)) and seismic data. For the definition of the seismic units and boundary reflectors, see text.

depth, a package of coal and siltstones is interbedded with the volcanic rocks. From the top of the volcanic section at 1,881 m depth up to c. 1,040 m depth, the lithology is predominantly cherty limestone, with sandy intervals at the bottom. A chalk interval is present between 1,040 and 911 m depth. Generally, unit U5 is characterized by upwards decreasing gamma ray values. There is high variability in the neutron density and sonic velocity logs in the section of volcanic rocks and the chalk section is characterized by an increase in neutron density and decrease in sonic velocity (Figure 7).

The NTC reflector, which forms the upper boundary of seismic unit U5, is situated at 925 m depth in Maastrichtian chalks. A sample at 911 m depth is the uppermost sample dated to the late Maastrichtian, while a sample retrieved at 908 m depth was dated to the early Paleocene. This would put the top of the Cretaceous section in the well between 908 and 911 m. It is also identified as a sharp change in the gamma ray, neutron porosity and sonic velocity logs (Figure 7).

The section between 911 m depth and the uppermost retrieved sample at 615 m depth, which corresponds to the lower part of seismic unit U4, is predominantly calcareous claystone, with some limestone interbeds near the bottom of the section and occasional sandy intervals throughout (Figure 7). The uppermost sample of late Paleocene age was sampled at 882 m depth. The youngest dated sample in the well was taken at a depth of 622 m and was dated to the early Eocene. Generally, the gamma ray values and sonic velocity decrease towards the top of this section, while neutron density increases.

The C30 and RD1 reflectors are both situated above the youngest dated sample, at 260 m depth and 120 m depth, respectively. The RD2 reflector would stratigraphically be placed in between these two reflectors but could not be traced from the study area to the location of the well.

5 Discussion

5.1 Chronostratigraphy

Several seismic lines in the dataset allow the seismic stratigraphy in the study area to be connected to the stratigraphy in the BMP, which was based on data from the IODP 307 boreholes (see Figure 1 for location; Van Rooij et al., 2003; Van Rooij et al., 2007a; Kano et al., 2007; Van Rooij et al., 2009). The data from well 62/7-1, as well as additional previously published work (McDonnell and Shannon, 2001; Stoker et al., 2001; Shannon et al., 2005), were used to determine the age of units and reflectors below the coring depth of the IODP 307 boreholes.

At the location of well 62/7-1, the basement reflector is situated in Bathonian-Bajocian rocks (Figure 7). The biostratigraphy data from the well demonstrate that the NTC reflector is Maastrichtian in age and situated near the top of the Late Cretaceous chalk section (Figure 7). Therefore, at this location, unit U5 is of Middle Jurassic to Late Cretaceous age.

As the C30 reflector is situated above the youngest dated sample in well 62/7-1 (Figure 7) and underneath the depth of the IODP 307 boreholes, its age cannot be determined from the well or borehole data. The large-scale undulating geometry and erosional

characteristics that it displays (Figure 2), however, are distinctive for the C30 reflector in the southern part of the Porcupine Basin (Shannon et al., 2005). Previous studies identifying this reflector were able to date it to the latest Eocene by linking seismic data to wells in the northern part of the basin (McDonnell and Shannon, 2001; Stoker et al., 2001). Consequently, unit U4 sediments are of Paleocene to Eocene age.
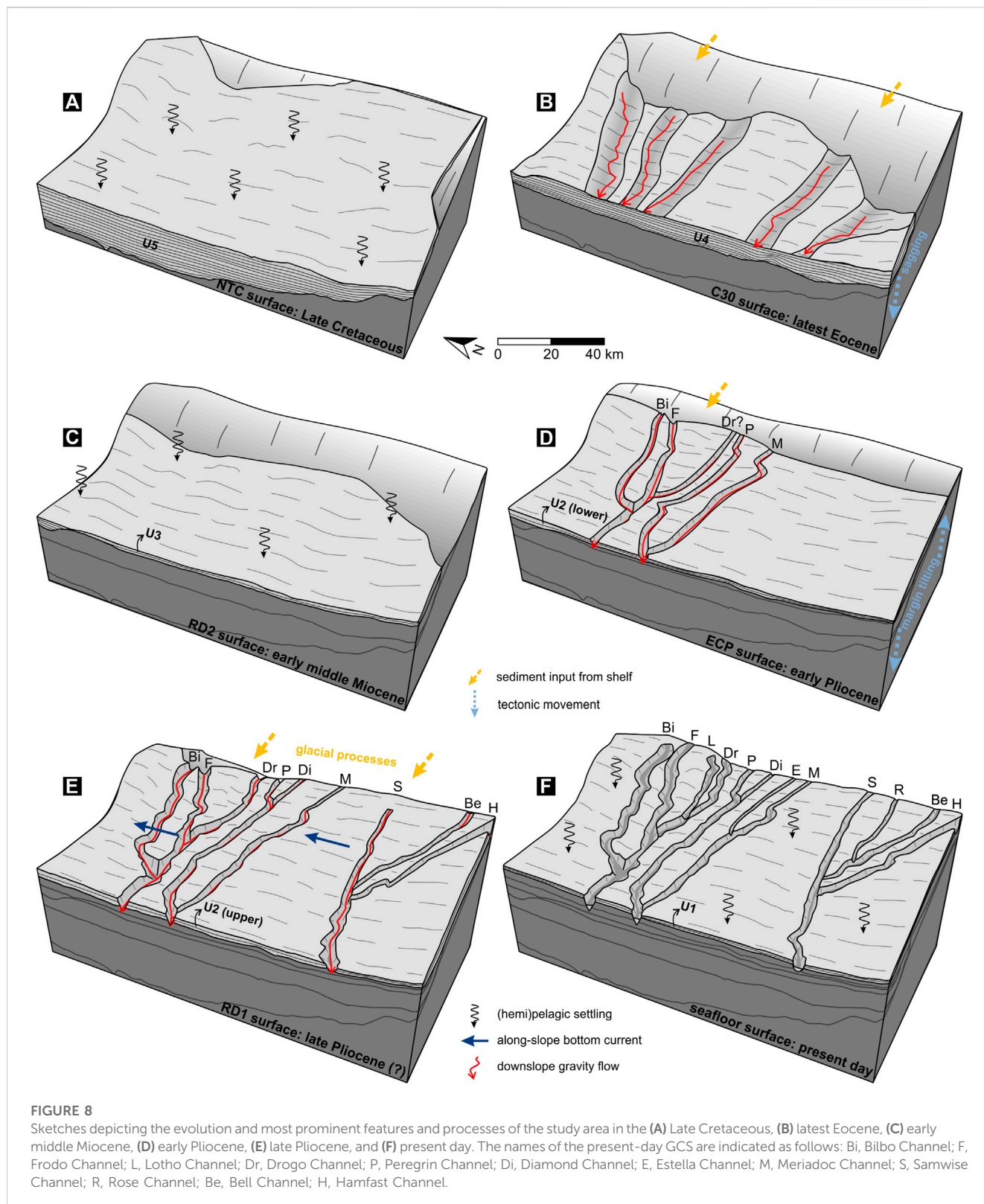
The RD2 reflector in the study area is the continuation of the RD2 reflector in the BMP and Kings Channel System (Van Rooij et al., 2003; Van Rooij et al., 2009; Verweirder et al., 2021). The reflector was dated to the early middle Miocene in IODP 307 borehole U1318 (Louwye et al., 2008), so unit U3 in the study area contains sediments of Oligocene to early Miocene age.

The RD1 reflector identified here is the continuation of the RD1 reflector in the BMP and Kings Channel System (Van Rooij et al., 2003; Van Rooij et al., 2009; Verweirder et al., 2021). The RD1 reflector was dated at IODP 307 site U1318, where it represents a hiatus between upper Miocene and upper Pliocene sediments (Kano et al., 2007). The erosive phase responsible for forming the RD1 reflector seems to have been extreme in the BMP (Van Rooij et al., 2007a), where strong bottom currents with local enhancement by tidal motions have been inferred from mooring data (Pingree and Le Cann, 1989; White, 2007). They removed (part of) the sediments below the RD1 horizon, causing a steep topography and a large hiatus (Van Rooij et al., 2003; White, 2007; Van Rooij et al., 2009). It is doubtful that the extent of this hiatus is consistent over the whole eastern margin of the Porcupine Seabight (Huvenne et al., 2009; Van Rooij et al., 2009). There is no indication for the presence of locally enhanced strong bottom currents here (Figure 2). Though the RD1 reflector is still erosional in places, its general conformability suggests less extreme current strengths and (non-) deposition rather than (extreme) erosion, which may indicate that it represents a smaller hiatus in the GCS than in the BMP. There is, therefore, no constraint on the exact age of the RD1 horizon (or the associated hiatus) in the study area at present. Due to a lack of precise age information in the study area, the seismic interpretation of the BMP at the IODP 307 sites is adopted here and sediments of unit U2 are tentatively attributed a middle Miocene to late Miocene/ Pliocene age.

The resumption of sedimentation after the RD1 erosion is variable, even over short distances (Huvenne et al., 2009). Cold-water coral mound frameworks promoting entrapment of particles allowed sedimentation as early as 2.7 Ma (Kano et al., 2007; Foubert and Henriet, 2009). In locations without such a framework to decrease bottom current intensity, sedimentation may not have resumed before 1.7 Ma (Kano et al., 2007; Huvenne et al., 2009). Therefore, unit U1 in the study area is thought to mainly consist of Quaternary sediments.

5.2 Processes and environments prior to GCS incision

The data at well 62/7-1 indicate that the seismic unit just above the acoustic basement (U5) consists of Jurassic calcareous claystones and igneous rocks underneath Cretaceous limestones and chalks (Figure 7). A coal-containing section interbedded with the igneous rocks suggests continental conditions at Goban Spur at the end of

FIGURE 8
Sketches depicting the evolution and most prominent features and processes of the study area in the **(A)** Late Cretaceous, **(B)** latest Eocene, **(C)** early middle Miocene, **(D)** early Pliocene, **(E)** late Pliocene, and **(F)** present day. The names of the present-day GCS are indicated as follows: Bi, Bilbo Channel; F, Frodo Channel; L, Lotho Channel; Dr, Drogo Channel; P, Peregrin Channel; Di, Diamond Channel; E, Estella Channel; M, Meriadoc Channel; S, Samwise Channel; R, Rose Channel; Be, Bell Channel; H, Hamfast Channel.

the Jurassic and several (very) calcareous sandy sections interbedded with limestones indicate a shallow and/or more dynamic marine depositional environment at the start of the Cretaceous. The upwards decreasing gamma values within the unit along with calcareous lithologies becoming more and more dominant (Figure 7) suggest a reducing terrigenous influence on deposition

and likely deepening of the basin. This is in accordance with the onset of thermal subsidence from the Early Cretaceous onwards (Shannon, 1991). Underneath the GCS, where the basin was deeper than at Goban Spur (Merlin Energy Resources Consortium, 2020), the (sub)parallel basin-filling reflections of seismic unit U5 (Figure 5A) are interpreted as an expression of low-energy

deposition in an open marine environment during the relatively warm Late Cretaceous (Figure 8A). This is in accordance with the presence of (very) calcareous lithologies on Goban Spur as well as previous work in the basin (McDonnell and Shannon, 2001; Stoker et al., 2017; Merlin Energy Resources Consortium, 2020).

Shannon et al. (1993) identified a last phase of chalk deposition in the Danian rocks in the Porcupine Basin that are not present in well 62/7-1, where the Cenozoic sequence starts with a section of younger-than-Danian calcareous claystones (Figure 7). This suggests the low-energy open marine setting of the Late Cretaceous persisted in the beginning of the Paleocene. The calcareous claystone section of the upper Paleocene and lower Eocene in well 62/7-1 shows that Goban Spur was not influenced by the deltaic sedimentary environment that developed in the northern part of the Porcupine Basin (Moore and Shannon, 1992). The seismic character of unit U4 in the study area with (sub)parallel reflections only occasionally and locally interrupted by internal erosion (Figure 5B) suggests it was predominantly governed by hemipelagic rather than deltaic processes. It was likely a marine basin environment, as also put forward by Merlin Energy Resources Consortium (2020). The large-scale incisions of the C30 reflector bounding the top of the unit indicate a period of major erosional impact from channelized gravity-driven clastic input, probably in the late Eocene as proposed by Shannon (1992) and McDonnell and Shannon (2001). This has been interpreted as a response to rapid differential subsidence (sagging) in the basin center causing steeper basin margin slopes (Praeg et al., 2005; Shannon et al., 2005; Figure 8B). In the study area, the C30 channels likely acted as a drainage system from the Celtic Sea Shelf into the basin as suggested by their orientation (Figure 3). They were part of a basin-wide Eocene system also including drainage from the northern and western edges of the basin to the center (Shannon, 1992; McDonnell and Shannon, 2001). Very similarly, an Eocene channel complex draining the continental margin off northwest Ireland was formed in the northeastern Rockall Basin and attributed to margin uplift (Georgiopoulou et al., 2021).

The upper Eocene to lowermost Miocene sedimentary sequence is above the sampled interval in well 62/7-1 (Figure 7) and below the depth that was reached in the IODP boreholes (Kano et al., 2007; Louwye et al., 2008). Well data in the northern Porcupine Basin, though, show that this sequence mainly consists of (calcareous) (silty to sandy) claystones (Merlin Energy Resources Consortium, 2020). In the Rockall Trough (see Figure 1 for location), contourite sequences have been recognized in seismic data at this level, which indicates the onset of deep-water circulation in an open marine setting created by a subsiding basin (Stoker, 1997; Praeg et al., 2005). In this scenario, the C30 reflector signifies the transition from a downslope dominated to an along-slope dominated sedimentation pattern (Stoker et al., 2001). As this reflector was also identified in the Porcupine Basin, the same interpretation was applied there (McDonnell and Shannon, 2001). However, the contourites in the Porcupine Basin are not as well developed and have so far only been described in the northern part of the basin (McDonnell and Shannon, 2001; Shannon et al., 2005). In the study area, seismic unit U3 has a relatively uniform thickness throughout (Figure 4C), and unit U3 reflectors are mostly parallel and mirror the C30 topography (Figure 2). This suggests draping and a predominantly hemipelagic sedimentary environment (Figure 8C). In the northernmost part of the study area though, the lower part of unit U3 is preferentially infilling one of the C30 paleochannels, onlapping the channel edges, while deposition on the adjacent high at this time was very thin or lacking (Figure 5C). This also suggests a hemipelagic environment dominated by

the settling of particles, though the preferential deposition in channels indicates some along-slope redistribution of sediments by bottom currents (cf. Georgiopoulou et al., 2021; Rodrigues et al., 2022). Reflectors on top of this C30 high are deposited predominantly after the channel infill (Figure 5) and their mounded geometry and low to moderate amplitude suggests bottom-current influence at the top of unit U3 (Rebesco et al., 2014). This concurs with observations in the BMP, where Miocene bottom currents have been inferred from the presence of wavy geometries underneath the RD2 reflector in sparker seismic data (Van Rooij et al., 2007a). A very similar though more developed succession of seismic facies has been described in the Rockall Trough, where interfluve areas are topographically amplified by the interaction of channel overbank and contouritic deposition (Georgiopoulou et al., 2021). Therefore, it appears that the contouritic signature is more subtle in the study area but increases northwards in the Porcupine basin and along the Irish margin of Rockall Trough. The subdued presence of upper Eocene-lowermost Miocene contourites in the Porcupine Seabight compared to the Rockall Trough has previously been attributed to the shape of the Porcupine Seabight and it being a more confined basin (McDonnell and Shannon, 2001). Thus, it was possibly less easily reached by deep-water currents compared to the open ocean setting of the Rockall Trough (McDonnell and Shannon, 2001).
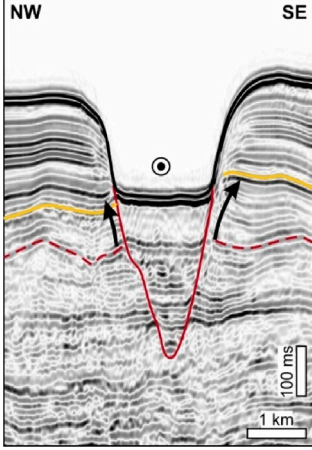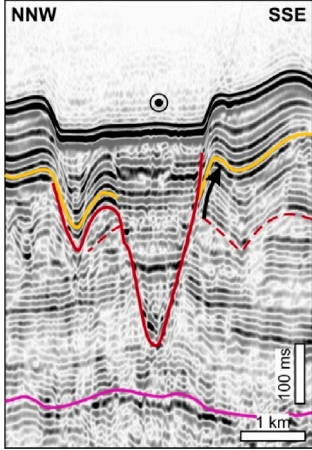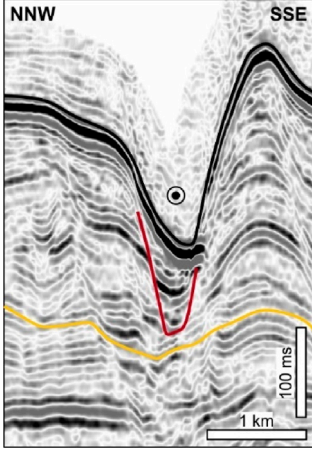
Data from IODP 307 show that deposition in the middle to late Miocene consisted of homogenous silty clays (Expedition 307 Scientists, 2006), suggesting a low-energy depositional environment. The reflectors of unit U2 are parallel and horizontal in the basin, suggesting hemipelagic deposition there. On the upper slope, however, reflectors in undulating configurations indicate the influence of bottom currents. A multitude of faults is present within unit U2, especially north of Bilbo Channel and between Meriadoc and Samwise channels (Figures 2, 5). These are similar to the polygonal faults described at the eastern edge of the Rockall Trough (Georgiopoulou et al., 2021), further accentuating the similarity of the processes occurring along the Irish margin.

5.3 Initial incision of the GCS

The distinct V shape and associated truncation of reflectors at the base of the GCS channels demonstrate that erosional downslope gravity flows are the driving mechanism for the formation of the system. A tentative timing of the initial incision can be deduced from the seismic data. The divergent reflections in unit U2 in proximity to the channel bases (Figure 6) are interpreted as levees suggestive of the presence of an adjacent channel. Levees are identified below the RD1 reflector in several places and next to several channels, indicating that the GCS was formed before the RD1 event. There are only a few locations where a channel base cuts through the RD2 reflector, and they do so only slightly, with the erosional edges continuing to a level above RD2. Therefore, the channels were formed sometime between the early middle Miocene (RD2) and the late Pliocene (RD1) (Figure 8D). This is contrary to what was previously proposed, and implies that the GCS was formed before the Kings Channel System just to the north (Van Rooij et al., 2009; Verweirder et al., 2021).
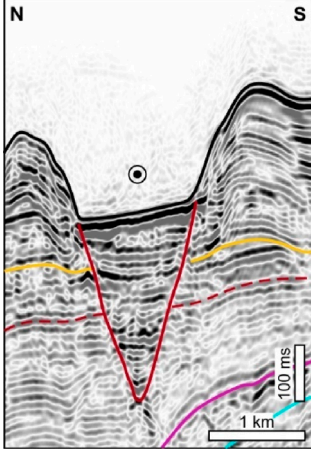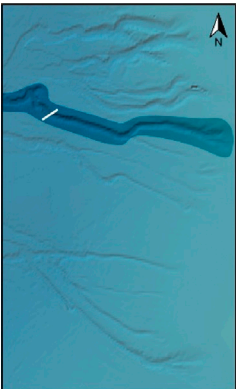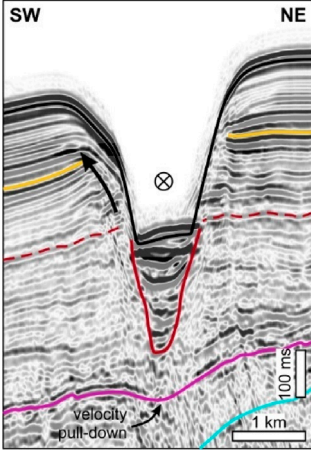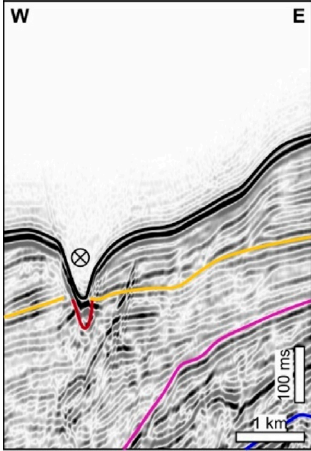
The ECP reflector is interpreted as a reflector representing early channel presence in the study area. It is situated at the base of clear levee formation on both sides of Peregrin Channel, and coincides with potential levee formation next to Bilbo, Frodo, and Meriadoc

TABLE 1 Table showing the location and seismic expression of the individual channels of the GCS used in this study. Colors used to indicate key reflectors and levee formation in the interpreted seismic data are the same as in Figure 2. Also shown are the inferred ages of the individual channels along with the arguments used in determining them. Lastly, the total depth of each channel (D: measured vertically from the shoulder to the deepest incision) and thickness of the channel infill (F: measured vertically from the seafloor to the deepest incision) is given as average [minimum-maximum] values.

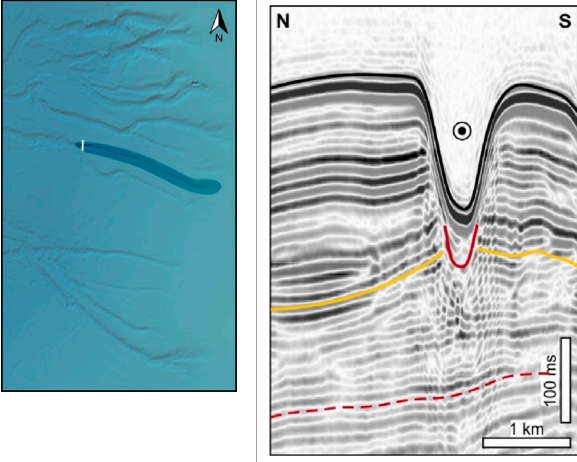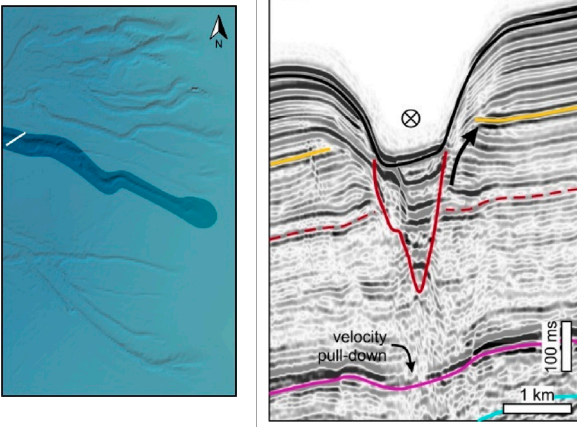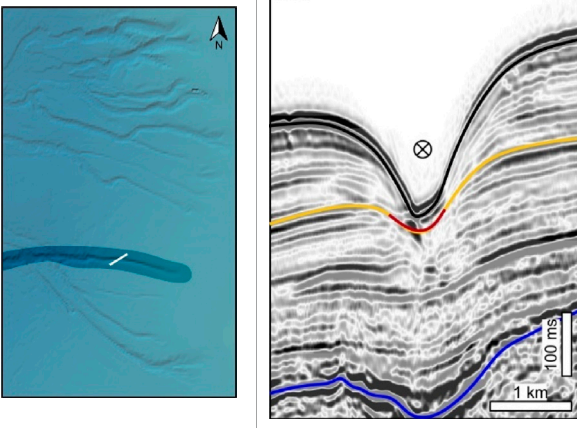| name + location	seismic expression	age	arguments	dimensions (s TWT)
Bilbo		early Pliocene (ECP reflector)	- levee formation - dipping reflectors that connect to the channel base are present below RD1	D: 0.58 [0.43-0.97] F: 0.32 [0.26-0.44]
Frodo		early Pliocene (ECP reflector)	levee formation	D: 0.45 [0.25-0.93] F: 0.27 [0.13-0.45]
Lotho		- younger than the four oldest channels - younger than late Pliocene (RD1 reflector)?	deepest incision does not reach down to the ECP reflector and in some profiles, it does not even reach down to the RD1 reflector	D: 0.33 [0.25-0.38] F: 0.13 [0.07-0.18]

(Continued on following page)

TABLE 1 (*Continued*) Table showing the location and seismic expression of the individual channels of the GCS used in this study. Colors used to indicate key reflectors and levee formation in the interpreted seismic data are the same as in Figure 2. Also shown are the inferred ages of the individual channels along with the arguments used in determining them. Lastly, the total depth of each channel (D: measured vertically from the shoulder to the deepest incision) and thickness of the channel infill (F: measured vertically from the seafloor to the deepest incision) is given as average [minimum-maximum] values.

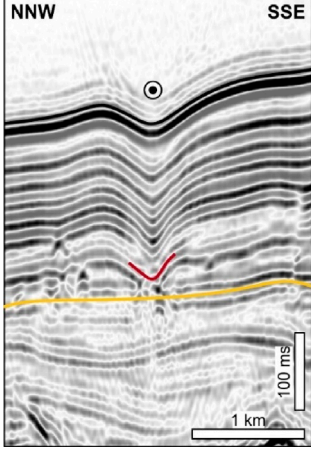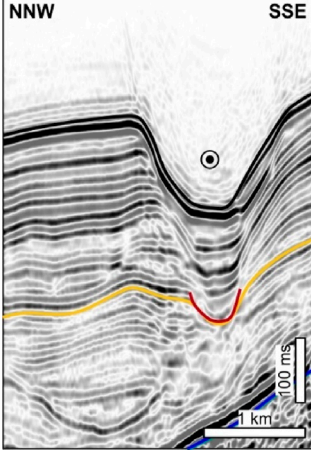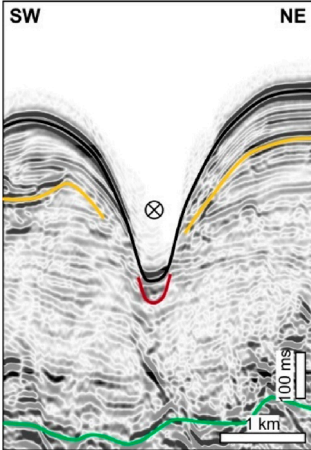| name + location	seismic expression	age	arguments	dimensions (s TWT)
Drogo		older than late Pliocene (RD1 reflector), but very unclear whether formed at the time of the ECP reflector or after	- deepest incision barely below the ECP reflector in one profile and completely above it in another, but very much below the ECP reflector in all other profiles - no levee identified though	D: 0.46 [0.41-0.58] F: 0.30 [0.18-0.42]
Peregrin		early Pliocene (ECP reflector)	levee formation	D: 0.45 [0.32-0.63] F: 0.22 [0.13-0.29]
Diamond		late Pliocene (RD1 reflector)?	- RD1 dips down and truncates reflectors underneath, where the facies shows continuity between both sides of the channel (Figure 5) - only two channel crossings, which increases uncertainty	D: 0.23 [0.14-0.33] F: 0.08 [0.00-0.17]

(Continued on following page)

TABLE 1 (*Continued*) Table showing the location and seismic expression of the individual channels of the GCS used in this study. Colors used to indicate key reflectors and levee formation in the interpreted seismic data are the same as in Figure 2. Also shown are the inferred ages of the individual channels along with the arguments used in determining them. Lastly, the total depth of each channel (D: measured vertically from the shoulder to the deepest incision) and thickness of the channel infill (F: measured vertically from the seafloor to the deepest incision) is given as average [minimum-maximum] values.

name + location	seismic expression	age	arguments	dimensions (s TWT)
Estella		younger than late Pliocene (RD1 reflector)	- deepest incision does not reach down below the RD1 reflector - only one channel crossing, which increases uncertainty	D: 0.22 [0.22-0.22] F: 0.06 [0.06-0.06]
Meriadoc		early Pliocene (ECP reflector)	levee formation	D: 0.39 [0.19-0.52] F: 0.20 [0.00-0.28]
Samwise		- older than late Pliocene (RD1 reflector)? - late Pliocene (RD1 reflector)?	- dipping reflectors connecting to the channel base seem present below RD1 in some profiles - in other profiles, RD1 seems to dip down and truncate reflectors underneath, where the facies shows continuity between both sides of the channel	D: 0.31 [0.23-0.41] F: 0.14 [0.00-0.26]

(Continued on following page)

TABLE 1 (*Continued*) Table showing the location and seismic expression of the individual channels of the GCS used in this study. Colors used to indicate key reflectors and levee formation in the interpreted seismic data are the same as in Figure 2. Also shown are the inferred ages of the individual channels along with the arguments used in determining them. Lastly, the total depth of each channel (D: measured vertically from the shoulder to the deepest incision) and thickness of the channel infill (F: measured vertically from the seafloor to the deepest incision) is given as average [minimum-maximum] values.

name + location	seismic expression	age	arguments	dimensions (s TWT)
Rose		younger than late Pliocene (RD1 reflector)	deepest incision does not reach down below the RD1 reflector	D: 0.04 [0.04-0.05] F: 0.00 [0.00-0.00]
Bell		late Pliocene (RD1 reflector)?	- RD1 reflector dips down at channel edges and truncates reflectors underneath, where the facies shows continuity between both sides of the channel	D: 0.29 [0.27-0.31] F: 0.13 [0.08-0.18]
Hamfast		late Pliocene (RD1 reflector)	- RD1 reflector dips down at channel edges and truncates reflectors underneath, where the facies shows continuity between both sides of the channel	D: 0.37 [0.21-0.47] F: 0.11 [0.00-0.26]

channels. This suggests synchronous (or near-synchronous) channel formation for these four channels, at least at the resolution of this dataset (Table 1). It is unclear whether Drogo Channel was formed at the same time as the four oldest channels, though down-dipping truncating reflectors do suggest it was present before the RD1 event (Table 1). The ECP reflector is situated deeper than the deepest point of

incision of Lotho and Estella channels, indicating these were formed later (Table 1). It is possible that a low in the RD1 topography was influential on the formation of Lotho Channel, but the dataset used here is insufficient to make a definite conclusion on the timing of formation of this channel. This is also the case for Estella Channel, as only one profile crosses the channel, though in this profile, the incision appears above the RD1 reflector (Table 1). The same uncertainty arises for Diamond Channel, where the two crossing profiles suggest the RD1 reflector may have been erosional and shaped the channel base (Table 1). Evidence for when the southern branches of the system were formed is even less clear. The ECP reflector is eroded by overlying reflectors before it reaches the southern branches, and tracing the RD1 reflector to the southern channels becomes increasingly difficult as well. Nevertheless, on several profiles, the facies underneath the RD1 reflector seems continuous on either side of Samwise Channel and truncating reflectors suggest channel formation at the time of the RD1 event (Table 1). However, the presence of potential levees and down-dipping truncating reflectors below the RD1 reflector are arguments for the formation of Samwise Channel before the RD1 event. Bell Channel and Hamfast Channel are likely younger than Samwise Channel and formed around the time of the RD1 event, shown by the presence of down-dipping truncating reflectors (Table 1). The incision of the smallest of the southern branches, Rose Channel, does not reach below the RD1 reflector, indicating this channel is younger than the RD1 event.

This discussion implies that five main channels (Bilbo, Frodo, Drogo, Peregrin, and Meriadoc) were formed well before the start of the Quaternary (RD1 event; Figure 8D). Several other channels (Diamond, Samwise, Bell, Hamfast, Lotho?) were formed later and likely just before or around the time the Quaternary started (Figure 8E), while at least some of the smaller channels (Estella, Rose) postdate the RD1 event and the start of the Quaternary (Figure 8F).

Quaternary glaciations on the Irish mainland and shelf (and associated lowered sea levels) were previously mentioned as probable sources of the sediment gravity flows that eroded the initial GCS thalwegs (Akhmetzhanov et al., 2003). The channels may indeed have been utilized and re-incised during deglaciation periods but the timing of the initial incision implies an earlier mechanism. The most likely scenario for initial incision of the system stems from passive margin tectonics. A phase of tilting across the NE Atlantic margin (from Norway to Ireland) in the early Pliocene (Stoker et al., 2005b; Praeg et al., 2005) has been associated with channel re-incision in the Rockall Trough (Elliott et al., 2006; Georgiopoulou et al., 2021), indicating the existence and erosive nature of downslope flows at the Irish margin at this time. Tilting includes uplift of onshore and shelfal areas producing source material, and coeval basin subsidence creating accommodation space (Praeg et al., 2005). Prograding clinoforms overlying an erosional surface, recognized as indicators of margin tilting further north (Dahlgren et al., 2005; Praeg et al., 2005), are here observed in unit U2 on the shelf edge (Figure 5). Additionally, prograding clinoforms were identified in middle to late Miocene seismic data on the Celtic Sea Shelf east of the channel heads (Merlin Energy Resources Consortium, 2020). This may indicate margin tilting and subsequent increased sediment supply to the shelf edge between the middle Miocene (RD2) and the late Pliocene (RD1) here as well, likely originating from the same early Pliocene episode. The tilting and likely associated erosive downslope flows are a possible explanation for the incision of the GCS channel bases and the timing of the tilting (between RD2 and RD1) is in agreement with the timing of incision of the first channels suggested before. However, a direct connection between the erosional surface on the outer shelf and the channels has not been observed.

Many of the channel bases of the present-day GCS seen on the seismic profiles are located above (the edges of) large depressions in the NTC, C30 and/or RD2 surfaces (Figures 2, 3). Within the section of the study area where the C30 reflector is present, 85% of the present-day GCS channels are located above a C30 paleochannel. The repetition of depressions in similar locations throughout time suggests that these have been preferential pathways for downslope sediment transport in the basin since the late Eocene and in some places perhaps since the end of the Cretaceous. Reoccupation of paleochannels leading to stacked channel fills is a known phenomenon in both terrestrial and marine settings (Elliott et al., 2006; Greene et al., 2007; Georgiopoulou et al., 2021; Horozal et al., 2021) and has been recreated in flume experiments (Reitz et al., 2010). A combination of greater compaction and higher erodibility of channel fill sediments compared to interfluve sediments has been suggested to create topographic lows over the paleochannels, thus favoring reincision at the same location later (Greene et al., 2007; Straub et al., 2009). However, different from these examples, the channels formed in the study area at the level of the C30 unconformity and subsequent lows at the level of the RD2 horizon are completely filled in during the late Paleogene-early Neogene. New channels are formed between the early middle Miocene (RD2) and the late Pliocene (RD1) by erosional downslope flows that did not simply reuse pre-existing depressions (Figure 8E). This is shown by quasi-horizontal reflectors just underneath and adjacent to the present-day GCS channel bases, with the bases cutting into those reflectors (Figures 2, 6). Therefore, erodibility and compaction of the paleochannel fills seem less likely to have influenced the location of incision of the present-day GCS. There are also no indications for a long-term tectonic influence on repeated flow pathways. Plenty of faults are present at several stratigraphic levels (Figures 2, 5), but it is difficult to recognize faults underneath the channels due to artefacts in the data. However, any faults that were tentatively identified only have small offsets and did not create abrupt changes in topography that would lead to preferential channel formation in those locations. Additionally, any large (reactivated) basin-bounding faults are oriented north-south and perpendicular to the orientation of the channel systems (Bailey et al., 2003). A combination of (small) lateral differences in seafloor lithology and topography at the time of incision is thought most likely to have influenced channel locations.

The repetitive presence of east-west oriented channels on the eastern slope of the Porcupine Seabight also indicates that there was a long-lived sediment source on the shelf intermittently providing sediment in gravity-driven flows. Both for the C30 paleochannels and the present-day channel system, passive margin tectonics (sagging and tilting, respectively) are seen as the main and most likely cause for increased sediment input (Praeg et al., 2005; Shannon et al., 2005). The characteristics of this source area are uncertain. The simplest interpretation would be a direct connection with a fluvial system on the Celtic Sea Shelf. While this is not apparent in the seismic data presented here or data on the shelf investigated in other studies (Giglio et al., 2022), well data may provide some arguments for this hypothesis. At the end of the Eocene, the outer shelf was a shallow marine environment but the

presence of late Eocene-early Oligocene paralic and fluvial facies on the inner Celtic Sea Shelf does suggest a narrower shelf than at present and closer proximity of terrestrial material (Merlin Energy Resources Consortium, 2020). In the early to middle Pleistocene, a fluvial to shallow marine facies with an unconformable base was deposited across the Celtic Sea Shelf (Merlin Energy Resources Consortium, 2020). It passes laterally into the open marine facies of the Porcupine basin, with the transition area on the outer shelf and upper slope near the GCS channel heads.

5.4 Channel processes

The evolution of the Gollum Channel System started with a canyon phase, where (possibly margin tilting-induced) erosive gravity flows produced V-shaped incisions (Figure 8D). Although the oldest major erosive episode has formed at least four of the channels simultaneously, the existence of younger channels implies multiple phases of incision, of which some around or after the time of the RD1 event (Figure 8E). Additionally, truncating reflectors at the channel edges above older channel bases suggest multiple phases of channel flank erosion after the initial incision, and especially after the late Pliocene (RD1; Figure 5C, 6). Although channel flank erosion could be due to the action of erosional bottom currents (Van Rooij et al., 2010; De Mol et al., 2011), the incision of additional channels points to several phases of re-activation of the source area. Even though glacially-derived turbidity currents are unlikely to have formed the oldest channels, they are the most likely source of sediment for the incision of new pathways after the RD1 event. The less extreme incisions of the younger channels indicate that these flows were less erosive than the flows that created the oldest channels. Some of these younger channels are later filled in and buried or draped and were seemingly active for only a short period of time (too close to larger channels causing spillover, possibly combined with sediment redirection by bottom currents), and some have eroded edges and seem to have been active for longer (Table 1).

Although many of the channels (especially the older ones) seem to have experienced repeated periods of activity over 5 Myr (Figure 6), the presence of a singular base and no lateral migration or visible re-incision suggests a single incision phase creating each of the channels. The distinct erosional phases after the initial incision suggest there were several moments in the Quaternary where the erosive nature of flows was such that they were capable of local flank erosion. Most of the downslope gravity flows entering any of the channels after their initial incision likely reused the newly created topography to flow into the Porcupine basin and either bypassed the upper slope or added to the channel fill.

Part of the sediment carried by the oldest incising gravity flows was deposited in the unit U2 levees on the channel edges. Levee growth is much reduced though not completely absent (e.g., Bilbo Channel) above the RD1 reflector, where draping dominates over active levee build-up. The (sub)horizontal, laterally continuous reflections of unit U1 suggest a dominance of hemipelagic processes (Figure 8F). However, there are several indications for along-slope bottom current action influencing deposition during the Quaternary.

Above the RD1 reflector, asymmetry in the levees is apparent in several channels, with a generally better-developed steeper northern levee and a smoother, less-developed southern levee (Figure 6). Levee asymmetry has also been described in several other canyon systems (Fuhrmann et al., 2020; Pandolpho et al., 2021) and was recreated in flume tank experiments (Miramontes et al., 2020). The phenomenon is attributed to along-slope oriented bottom currents interfering with downslope-oriented gravity flows, with increased bottom current velocities leading to increased levee asymmetry (Miramontes et al., 2020). The levee on the downstream side of the bottom current is better developed (wider, more bedforms) due to more overspill there and inhibition of overspill by the bottom current on the upstream channel edge (Miramontes et al., 2020). Additionally, the downstream channel flank may act as an obstacle to the bottom currents, causing erosion there and draping on the upstream channel flank (Van Rooij et al., 2010; De Mol et al., 2011). The evolution from symmetry in the U2 levees (especially visible in Peregrin and Meriadoc channels) to levee asymmetry above RD1 suggests little to no bottom current influence on the GCS in its early stages, and slightly higher influence from a northward-flowing bottom current from the RD1 event onwards (Figure 8E). This is in agreement with the introduction of the Mediterranean Outflow Water into the Porcupine Seabight at the time of the RD1 event. This water mass is carried northwards along the eastern slope of the basin by the European Slope Current and produces enhanced bottom currents through interaction with over- and underlying water masses (Van Rooij et al., 2003; Toucanne et al., 2021). The levees disappear towards the top of unit U1 (Figure 6; Verweirder et al., 2021), indicating that the channels evolved to accommodate any flows running through them towards the end of the Quaternary. By this time, flows may have been completely contained within the channels, too infrequent, or not carrying big sediment loads.

5.5 Regional importance

There was little to no interaction with bottom currents in the initial stages of GCS existence. When the Mediterranean Outflow Water was introduced in the basin, downslope-transported sediment was thieved by northerly along-slope bottom currents. Thus, even though the channel system was formed before, the oceanographic conditions allowed sediment transport to the BMP from the start of the Quaternary at the earliest. During glacial periods, bottom currents slowed down, reducing the potential for sediment to be brought north to the BMP. Periods of deglaciation, on the other hand, caused increased sediment input into the GCS, with some gravity flows capable of eroding new pathways (and formation of a whole new channel system: the Kings Channel System; Verweirder et al., 2021). Additionally, bottom current strength picked up as climatic conditions changed, potentially allowing thieving of sediments and nutrients from the channels for drift and coral mound build-up in the BMP. This process was likely halted when the channels became deep enough to accommodate flows running through them, inhibiting the thieving of sediments by bottom currents. The increasing importance of hemipelagic processes over bottom current-related deposition throughout the Quaternary visible in the GCS is also seen

in the last 0.5 Myr in the BMP; glacial deposition with some muddy contourites is favored over coral growth and mound development (Huvenne et al., 2009).

The GCS is here proposed to have been the conduit for downslope sediment transport into the Porcupine Seabight since the early Pliocene. If it was indeed fed by a fluvial system on the Celtic Sea Shelf, this might explain its initial likeness to the Bay of Biscay canyons, which were fed by the Fleuve Manche paleoriver (Bourillet et al., 2003; Toucanne et al., 2009; Toucanne et al., 2012). A subsequent lower amount of sediment input and/or less erosive nature of downslope gravity flows in the Quaternary is a likely reason for the present-day difference between the GCS and the canyons in the Bay of Biscay. In this regard, oceanographic processes on the shelf (wind-driven currents and downwelling circulation between shelf and slope) and upper slope (internal tides) are potentially crucial (Heijnen et al., 2022).

6 Conclusion

From the seismic reflection data and well data presented here, it is inferred that the Gollum Channel System in the Porcupine Seabight was formed by basin margin tilting in the Pliocene. It is also shown that while all of the channels visible in the present-day bathymetry have a long history, they were not all formed at the same time. Some, the smaller ones, were formed in the Quaternary, likely by the erosive action of gravity flows related to glacial processes. The lack of lateral migration and the presence of a singular base in all channels points to one incision phase creating each channel. After the first incision phase in the Pliocene, there were a few subsequent moments where gravity flows were capable of (re-) incision and less extreme (channel flank) erosion. They likely mostly followed the pre-existing topography and either bypassed the upper slope or contributed to the channel fill.

The present-day channel system is underlain by an infilled and buried latest Eocene channel system, suggesting these conduits have been preferential pathways for downslope sediment transport on different occasions. There does not seem to be any structural control on the pathways, and the main influence on the location of the channels is thought to be (small-scale) pre-existing variability in bathymetry.

The influence of large-scale canyon-channel systems as sediment conduits on depositional systems and habitats elsewhere in a basin is illustrated by the link between activity in the GCS and depositional regimes in the BMP. The interaction with thieving along-slope bottom currents is crucial and enlarges the area of influence of the channel system significantly. These are processes that should also be considered and better understood in light of the distribution of terrestrially-derived pollutants.

Data availability statement

The data analyzed in this study is subject to the following licenses/restrictions: The seismic and well data included in this manuscript are copyright of the Government of Ireland and were provided under Data Licence Agreement by the Department of the Environment, Climate and Communications. Requests to access these datasets should be

directed to the Department of the Environment, Climate and Communications, customer.service@decc.gov.ie.

Author contributions

LV: Conceptualization, Funding acquisition, Investigation, Methodology, Visualization, Writing–original draft, Writing–review and editing. DV: Conceptualization, Funding acquisition, Project administration, Supervision, Writing–review and editing. AG: Conceptualization, Supervision, Writing–review and editing.

Funding

Acknowledgments

Conflict of interest

Author AG was employed by Ternan Energy.

The remaining authors declare that the research was conducted in the absence of any commercial or financial relationships that could be construed as a potential conflict of interest.

Publisher's note

All claims expressed in this article are solely those of the authors and do not necessarily represent those of their affiliated organizations, or those of the publisher, the editors and the reviewers. Any product that may be evaluated in this article, or claim that may be made by its manufacturer, is not guaranteed or endorsed by the publisher.

Supplementary material

The Supplementary Material for this article can be found online at: https://www.frontiersin.org/articles/10.3389/feart.2023.1285171/full#supplementary-material

SUPPLEMENTARY FIGURE S1
Velocity model used for the time-depth conversion at the location of well 62/7-1. The depths of boundary reflectors seafloor, RD1, C30, NTC and basement are also shown, as well as the depth of the uppermost early Eocene and early Paleocene samples.

References

Akhmetzhanov, A., Kenyon, N. H., Ivanov, M., and Cronin, B. T. (2003). "The continental Rise west of porcupine Seabight, Northeast Atlantic," in *European margin sediment dynamics: side-scan sonar and seismic images*. Editors J. Mienert and P. Weaver (Springer Science & Business Media), 187–192.

Amaro, T., Huvenne, V. A. I., Allcock, A. L., Aslam, T., Davies, J. S., Danovaro, R., et al. (2016). The Whittard Canyon – a case study of submarine canyon processes. *Prog. Oceanogr.* 146, 38–57. doi:10.1016/j.pocean.2016.06.003

Aslam, T., Hall, R. A., and Dye, S. R. (2018). Internal tides in a dendritic submarine canyon. *Prog. Oceanogr.* 169, 20–32. doi:10.1016/j.pocean.2017.10.005

Babonneau, N., Delacourt, C., Cancouët, R., Sisavath, E., Bachèlery, P., Mazuel, A., et al. (2013). Direct sediment transfer from land to deep-sea: insights into shallow multibeam bathymetry at La Réunion Island. *Mar. Geol.* 346, 47–57. doi:10.1016/j.margeo.2013.08.006

Bailey, W., Shannon, P. M., Walsh, J. J., and Unnithan, V. (2003). The spatial distributions of faults and deep sea carbonate mounds in the Porcupine Basin, offshore Ireland. *Mar. Pet. Geol.* 20, 509–522. doi:10.1016/S0264-8172(03)00079-5

Bourillet, J. F., Reynaud, J.-Y., Baltzer, A., and Zaragosi, S. (2003). The "Fleuve Manche": the submarine sedimentary features from the outer shelf to the deep-sea fans. *J. Quat. Sci.* 18, 261–282. doi:10.1002/jqs.757

Canals, M., Puig, P., Durrieu de Madron, X., Heussner, S., Palanques, A., and Fabres, J. (2006). Flushing submarine canyons. *Nature* 444, 354–357. doi:10.1038/nature05271

Dahlgren, K. I. T., Vorren, T. O., Stoker, M. S., Nielsen, T., Nygård, A., and Sejrup, H. P. (2005). Late Cenozoic prograding wedges on the NW European continental margin: their formation and relationship to tectonics and climate. *Mar. Pet. Geol.* 22, 1089–1110. doi:10.1016/j.marpetgeo.2004.12.008

Daly, E., Johnson, M. P., Wilson, A. M., Gerritsen, H. D., Kiriakoulakis, K., Allcock, A. L., et al. (2018). Bottom trawling at Whittard Canyon: evidence for seabed modification, trawl plumes and food source heterogeneity. *Prog. Oceanogr.* 169, 227–240. doi:10.1016/j.pocean.2017.12.010

De Mol, L., Van Rooij, D., Pirlet, H., Greinert, J., Frank, N., Quemmerais, F., et al. (2011). Cold-water coral habitats in the penmarc'h and guilvinec canyons (Bay of Biscay): deep-water versus shallow-water settings. *Mar. Geol.* 282, 40–52. doi:10.1016/j.margeo.2010.04.011

Department of Communications, Energy and Natural Resources (2010). The online integrated petroleum affairs system (IPAS). http://gis.dcenr.gov.ie/internetIPAS/servlet/internet/IPAS2IHome (Accessed October 6, 2023).

Elliott, G. M., Shannon, P. M., Haughton, P. D. W., Praeg, D., and O'Reilly, B. (2006). Mid-to Late Cenozoic canyon development on the eastern margin of the Rockall Trough, offshore Ireland. *Mar. Geol.* 229, 113–132. doi:10.1016/j.margeo.2006.03.008

Expedition 307 Scientists (2006). "Site U1318," in *Proc. IODP*, 307. doi:10.2204/iodp.proc.307.105.2006

Foubert, A., and Henriet, J.-P. (2009). in *Nature and significance of the recent carbonate mound record: the Mound Challenger Code*. Editors J. Reitner, M. H. Trauth, K. Stüwe, and D. Yuen (Springer Science & Business Media).

Fuhrmann, A., Kane, I. A., Clare, M. A., Ferguson, R. A., Schomacker, E., Bonamini, E., et al. (2020). Hybrid turbidite-drift channel complexes: an integrated multiscale model. *Geology* 48, 562–568. doi:10.1130/G47179.1

Georgiopoulou, A., Owens, M., and Haughton, P. D. W. (2021). Channel and inter-channel morphology resulting from the long-term interplay of alongslope and downslope processes, NE Rockall Trough, NE Atlantic. *Mar. Geol.* 441, 106624. doi:10.1016/j.margeo.2021.106624

Giglio, C., Benetti, S., Sacchetti, F., Lockhart, E., Clarke, J. H., Plets, R., et al. (2022). A Late Pleistocene channelized subglacial meltwater system on the Atlantic continental shelf south of Ireland. *Boreas* 51, 118–135. doi:10.1111/bor.12536

Greene, D. L., Jr., Rodriguez, A. B., and Anderson, J. B. (2007). Seaward-branching coastal-plain and piedmont incised-valley systems through multiple sea-level cycles: late Quaternary examples from Mobile Bay and Mississippi Sound. *U.S.A. J. Sed. Res.* 77, 139–158. doi:10.2110/jsr.2007.016

Hall, R. A., Aslam, T., and Huvenne, V. A. I. (2017). Partly standing internal tides in a dendritic submarine canyon observed by an ocean glider. *Deep. Res. Part I Oceanogr. Res. Pap.* 126, 73–84. doi:10.1016/j.dsr.2017.05.015

Harris, P. T., and Whiteway, T. (2011). Global distribution of large submarine canyons: geomorphic differences between active and passive continental margins. *Mar. Geol.* 285, 69–86. doi:10.1016/j.margeo.2011.05.008

Heijnen, M. S., Mienis, F., Gates, A. R., Bett, B. J., Hall, R. A., Hunt, J., et al. (2022). Challenging the highstand-dormant paradigm for land-detached submarine canyons. *Nat. Commun.* 13, 1–11. doi:10.1038/s41467-022-31114-9

Horozal, S., Chae, S., Seo, J. M., Lee, S. M., Han, H. S., Cukur, D., et al. (2021). Quaternary evolution of the southeastern Korean continental shelf, East Sea: paleo-incised valley and channel systems. *Mar. Petrol. Geol.* 128, 105011. doi:10.1016/j.marpetgeo.2021.105011

Huvenne, V. A. I., Van Rooij, D., De Mol, B., Thierens, M., O'Donnell, R., and Foubert, A. (2009). Sediment dynamics and palaeo-environmental context at key stages in the Challenger cold-water coral mound formation: clues from sediment deposits at the mound base. *Deep. Res. Part I Oceanogr. Res. Pap.* 56, 2263–2280. doi:10.1016/j.dsr.2009.08.003

Jenson, S. K., and Domingue, J. O. (1988). Extracting topographic structure from digital elevation data for geographic information system analysis. *Photogramm. Eng. Remote Sens.* 54, 1593–1600.

Kano, A., Ferdelman, T. G., Williams, T., Henriet, J.-P., Ishikawa, T., Kawagoe, N., et al. (2007). Age constraints on the origin and growth history of a deep-water coral mound in the northeast Atlantic drilled during Integrated Ocean Drilling Program Expedition 307. *Geology* 35, 1051–1054. doi:10.1130/G23917A.1

Kenyon, N. H., Belderson, R. H., and Stride, A. H. (1978). Channels, canyons and slump folds on the continental slope between South-West lreland and Spain. *Oceanol. Acta* 1, 369–380.

Khripounoff, A., Crassous, P., Lo Bue, N., Dennielou, B., and Silva Jacinto, R. (2012). Different types of sediment gravity flows detected in the Var submarine canyon (northwestern Mediterranean Sea). *Prog. Oceanogr.* 106, 138–153. doi:10.1016/j.pocean.2012.09.001

Louwye, S., Foubert, A., Mertens, K., Van Rooij, D., and The IODP Expedition 307 Scientific Party (2008). Integrated stratigraphy and palaeoecology of the lower and middle Miocene of the Porcupine Basin. *Geol. Mag.* 145, 321–344. doi:10.1017/S0016756807004244

Martín, J., Puig, P., Palanques, A., and Ribó, M. (2014). Trawling-induced daily sediment resuspension in the flank of a Mediterranean submarine canyon. *Deep. Res. Part II Top. Stud. Oceanogr.* 104, 174–183. doi:10.1016/j.dsr2.2013.05.036

McCann, T., Shannon, P. M., and Moore, J. G. (1995). Fault styles in the Porcupine Basin, offshore Ireland: tectonic and sedimentary controls. *Geol. Soc. Lond. Spec. Publ.* 93, 371–383. doi:10.1144/gsl.sp.1995.093.01.29

McDonnell, A., and Shannon, P. M. (2001). Comparative tertiary stratigraphic evolution of the porcupine and Rockall basins. *Geol. Soc. Lond. Spec. Publ.* 188, 323–344. doi:10.1144/GSL.SP.2001.188.01.19

Merlin Energy Resources Consortium (2020). The standard stratigraphic nomenclature of offshore Ireland: an integrated lithostratigraphic, biostratigraphic and sequence stratigraphic framework. Project atlas. *Pet. Aff. Div. Dep. Commun. Clim. Action environ. Spec. Publ.*

Miramontes, E., Eggenhuisen, J. T., Jacinto, R. S., Poneti, G., Pohl, F., Normandeau, A., et al. (2020). Channel-levee evolution in combined contour current-turbidity current flows from flume-tank experiments. *Geology* 48, 353–357. doi:10.1130/G47508C.1

Moore, J. G., and Shannon, P. M. (1992). Palaeocene-Eocene deltaic sedimentation, Porcupine Basin, offshore Ireland - a sequence stratigraphic approach. *First Break* 10, 461–469. doi:10.3997/1365-2397.1992024

Mountjoy, J. J., Micallef, A., Stevens, C. L., and Stirling, M. W. (2014). Holocene sedimentary activity in a non-terrestrially coupled submarine canyon: cook Strait Canyon system, New Zealand. *Deep. Res. Part II Top. Stud. Oceanogr.* 104, 120–133. doi:10.1016/j.dsr2.2013.09.001

Mulder, T., Zaragosi, S., Garlan, T., Mavel, J., Cremer, M., Sottolichio, A., et al. (2012). Present deep-submarine canyons activity in the Bay of Biscay (NE atlantic). *Mar. Geol.* 295–298, 113–127. doi:10.1016/j.margeo.2011.12.005

Naylor, D., and Shannon, P. M. (2005). "The structural framework of the Irish Atlantic Margin," in *Petroleum geology: north-west europe and global perspectives - proceedings of the 6th petroleum geology conference*. Editors A. G. Doré and B. A. Vining (London: Geological Society), 1009–1021.

Pandolpho, B. T., da Fontoura Klein, A. H., Dutra, I., Mahiques, M. M., Viana, A. R., Bueno, G. V., et al. (2021). Seismic record of a cyclic turbidite-contourite system in the Northern Campos Basin, SE Brazil. *Mar. Geol.* 434, 106422. doi:10.1016/j.margeo.2021.106422

Pingree, R. D., and Le Cann, B. (1989). Celtic and Armorican slope and shelf residual currents. *Prog. Oceanogr.* 23, 303–338. doi:10.1016/0079-6611(89)90003-7

Praeg, D., Stoker, M. S., Shannon, P. M., Ceramicola, S., Hjelstuen, B., Laberg, J. S., et al. (2005). Episodic Cenozoic tectonism and the development of the NW European "passive" continental margin. *Mar. Pet. Geol.* 22, 1007–1030. doi:10.1016/j.marpetgeo.2005.03.014

Puig, P., Ogston, A. S., Mullenbach, B. L., Nittrouer, C. A., Parsons, J. D., and Sternberg, R. W. (2004). Storm-induced sediment gravity flows at the head of the Eel submarine canyon, northern California margin. *J. Geophys. Res. Ocean.* 109, 1–10. doi:10.1029/2003jc001918

Puig, P., Greenan, B. J. W., Li, M. Z., Prescott, R. H., and Piper, D. J. W. (2013). Sediment transport processes at the head of Halibut Canyon, eastern Canada margin: an interplay between internal tides and dense shelf-water cascading. *Mar. Geol.* 341, 14–28. doi:10.1016/j.margeo.2013.05.004

Puig, P., Durán, R., Muñoz, A., Elvira, E., and Guillén, J. (2017). Submarine canyon-head morphologies and inferred sediment transport processes in the Alías-Almanzora canyon system (SW Mediterranean): on the role of the sediment supply. *Mar. Geol.* 393, 21–34. doi:10.1016/j.margeo.2017.02.009

Rebesco, M., Hernández-Molina, F. J., Van Rooij, D., and Wåhlin, A. (2014). Contourites and associated sediments controlled by deep-water circulation processes: State-of-the-art and future considerations. *Mar. Geol.* 352, 111–154. doi:10.1016/j.margeo.2014.03.011

Reitz, M. D., Jerolmack, D. J., and Swenson, J. B. (2010). Flooding and flow path selection on alluvial fans and deltas. *Geophys. Res. Lett.* 37, L06401. doi:10.1029/2009GL041985

Rise, L., Bøe, R., Riis, F., Bellec, V. K., Laberg, J. S., Eidvin, T., et al. (2013). The Lofoten-Vesterålen continental margin, North Norway: canyons and mass-movement activity. *Mar. Pet. Geol.* 45, 134–149. doi:10.1016/j.marpetgeo.2013.04.021

Rodrigues, S., Deptuck, M. E., Kendell, K. L., Campbell, C., and Hernández-Molina, F. J. (2022). Cretaceous to Eocene mixed turbidite-contourite systems offshore Nova Scotia (Canada): spatial and temporal variability of down- and along-slope processes. *Mar. Pet. Geol.* 138, 105572. doi:10.1016/j.marpetgeo.2022.105572

Shannon, P. M., Moore, J. G., Jacob, A. W. B., and Makris, J. (1993). Cretaceous and Tertiary basin development west of Ireland. *Petroleum Geol. North West Eur. Proc. Fourth Conf.*, 1057–1066. doi:10.1144/0041057

Shannon, P. M., Stoker, M. S., Praeg, D., van Weering, T. C. E., de Haas, H., Nielsen, T., et al. (2005). Sequence stratigraphic analysis in deep-water, underfilled NW European passive margin basins. *Mar. Pet. Geol.* 22, 1185–1200. doi:10.1016/j.marpetgeo.2005.03.013

Shannon, P. M., McDonnell, A., and Bailey, W. R. (2007). The evolution of the Porcupine and Rockall basins, offshore Ireland: the geological template for carbonate mound development. *Int. J. Earth Sci.* 96, 21–35. doi:10.1007/s00531-006-0081-y

Shannon, P. M. (1991). The development of Irish offshore sedimentary basins. *J. Geol. Soc. Lond.* 148, 181–189. doi:10.1144/gsjgs.148.1.0181

Shannon, P. M. (1992). Early Tertiary submarine fan deposits in the Porcupine Basin, offshore Ireland. *Geol. Soc. Spec. Publ.* 62, 351–373. doi:10.1144/GSL.SP.1992.062.01.27

Stoker, M. S., Van Weering, T. C. E., and Svaerdborg, T. (2001). A mid-to late cenozoic tectonostratigraphic framework for the Rockall Trough. *Geol. Soc. Lond. Spec. Publ.* 188, 411–438. doi:10.1144/GSL.SP.2001.188.01.26

Stoker, M. S., Praeg, D., Hjelstuen, B. O., Laberg, J. S., Nielsen, T., and Shannon, P. M. (2005a). Neogene stratigraphy and the sedimentary and oceanographic development of the NW European Atlantic margin. *Mar. Pet. Geol.* 22, 977–1005. doi:10.1016/j.marpetgeo.2004.11.007

Stoker, M. S., Praeg, D., Shannon, P. M., Hjelstuen, B. O., Laberg, J. S., Nielsen, T., et al. (2005b). Neogene evolution of the atlantic continental margin of NW europe (lofoten islands to SW Ireland): anything but passive. *Pet. Geol. Conf. Proc.*, 1057–1076. doi:10.1144/0061057

Stoker, M. S., Stewart, M. A., Shannon, P. M., Bjerager, M., Nielsen, T., Blischke, A., et al. (2017). An overview of the upper palaeozoic – mesozoic stratigraphy of the NE atlantic region. *Geol. Soc. Lond. Spec. Publ.* 447, 11–68. doi:10.1144/SP447.2

Stoker, M. S. (1997). Mid-to late Cenozoic sedimentation on the continental margin off NW Britain. *J. Geol. Soc. Lond.* 154, 509–515. doi:10.1144/gsjgs.154.3.0509

Straub, K. M., Paola, C., Mohrig, D., Wolinsky, M. A., and George, T. (2009). Compensational stacking of channelized sedimentary deposits. *J. Sed. Res.* 79, 673–688. doi:10.2110/jsr.2009.070

Thierens, M., Pirlet, H., Colin, C., Latruwe, K., Vanhaecke, F., Lee, J. R., et al. (2012). Ice-rafting from the British-Irish ice sheet since the earliest Pleistocene (2.6 million years ago): implications for long-term mid-latitudinal ice-sheet growth in the North Atlantic region. *Quat. Sci. Rev.* 44, 229–240. doi:10.1016/j.quascirev.2010.12.020

Toucanne, S., Zaragosi, S., Bourillet, J. F., Naughton, F., Cremer, M., Eynaud, F., et al. (2008). Activity of the turbidite levees of the Celtic-Armorican margin (Bay of Biscay) during the last 30,000 years: imprints of the last European deglaciation and Heinrich events. *Mar. Geol.* 247, 84–103. doi:10.1016/j.margeo.2007.08.006

Toucanne, S., Zaragosi, S., Bourillet, J. F., Gibbard, P. L., Eynaud, F., Giraudeau, J., et al. (2009). A 1.2 Ma record of glaciation and fluvial discharge from the West European Atlantic margin. *Quat. Sci. Rev.* 28, 2974–2981. doi:10.1016/j.quascirev.2009.08.003

Toucanne, S., Zaragosi, S., Bourillet, J.-F., Dennielou, B., Jorry, S. J., Jouet, G., et al. (2012). External controls on turbidite sedimentation on the glacially-influenced Armorican margin (Bay of Biscay, western European margin). *Mar. Geol.* 303–306, 137–153. doi:10.1016/j.margeo.2012.02.008

Toucanne, S., Soulet, G., Riveiros, N. V., Boswell, S. M., Dennielou, B., Waelbroeck, C., et al. (2021). The North atlantic glacial eastern boundary current as a key driver for ice-sheet—AMOC interactions and climate instability. *Paleoceanogr. Paleoclimatology* 36, e2020PA004068. doi:10.1029/2020PA004068

Tudhope, A. W., and Scoffin, T. P. (1995). Processes of sedimentation in Gollum Channel, porcupine Seabight: submersible observations and sediment analyses. *Trans. R. Soc. Edinb. Earth Sci.* 86, 49–55. doi:10.1017/S0263593300002157

Van Rooij, D., De Mol, B., Huvenne, V. A. I., Ivanov, M. K., and Henriet, J.-P. (2003). Seismic evidence of current-controlled sedimentation in the Belgica mound province, upper Porcupine slope, southwest of Ireland. *Mar. Geol.* 195, 31–53. doi:10.1016/s0025-3227(02)00681-3

Van Rooij, D., Blamart, D., Kozachenko, M., and Henriet, J.-P. (2007a). Small mounded contourite drifts associated with deep-water coral banks, Porcupine Seabight, NE Atlantic Ocean. *Geol. Soc. Lond. Spec. Publ.* 276, 225–244. doi:10.1144/gsl.sp.2007.276.01.11

Van Rooij, D., Blamart, D., Richter, T., Wheeler, A. J., Kozachenko, M., and Henriet, J.-P. (2007b). Quaternary sediment dynamics in the Belgica mound province, Porcupine Seabight: ice-rafting events and contour current processes. *Int. J. Earth Sci.* 96, 121–140. doi:10.1007/s00531-006-0086-6

Van Rooij, D., Huvenne, V. A. I., Blamart, D., Henriet, J.-P., Wheeler, A. J., and de Haas, H. (2009). The Enya mounds: a lost mound-drift competition. *Int. J. Earth Sci.* 98, 849–863. doi:10.1007/s00531-007-0293-9

Van Rooij, D., De Mol, L., Le Guilloux, E., Wisshak, M., Huvenne, V. A. I., Moeremans, R., et al. (2010). Environmental setting of deep-water oysters in the Bay of Biscay. *Deep. Res. Part I Oceanogr. Res. Pap.* 57, 1561–1572. doi:10.1016/j.dsr.2010.09.002

Van Rooij, D. (2004). *An integrated study of Quaternary sedimentary processes on the eastern slope of the Porcupine Seabight, SW of Ireland*. Unpubl. Dr. Diss. Ghent Univ. Belgium.

Verweirder, L., Van Rooij, D., White, M., Van Landeghem, K., Bossée, K., and Georgiopoulou, A. (2021). Combined control of bottom and turbidity currents on the origin and evolution of channel systems, examples from the Porcupine Seabight. *Mar. Geol.* 442, 106639. doi:10.1016/j.margeo.2021.106639

Voigt, I., Henrich, R., Preu, B. M., Piola, A. R., Hanebuth, T. J. J., Schwenk, T., et al. (2013). A submarine canyon as a climate archive - interaction of the Antarctic Intermediate Water with the Mar del Plata Canyon (Southwest Atlantic). *Mar. Geol.* 341, 46–57. doi:10.1016/j.margeo.2013.05.002

Waterhouse, A. F., Mackinnon, J. A., Musgravea, R. C., Kelly, S. M., Pickering, A., and Nash, J. (2017). Internal tide convergence and mixing in a submarine canyon. *J. Phys. Oceanogr.* 47, 303–322. doi:10.1175/JPO-D-16-0073.1

Weaver, P. P. E., Wynn, R. B., Kenyon, N. H., and Evans, J. (2000). Continental margin sedimentation, with special reference to the north-east Atlantic margin. *Sedimentology* 47, 239–256. doi:10.1046/j.1365-3091.2000.0470s1239.x

Wheeler, A. J. A. J., Kenyon, N. H. N. H., Ivanov, M. K., Beyer, A., Cronin, B. T. B. T., Schenke, H. W., et al. (2003). "Canyon heads and channel architecture of the Gollum Channel, porcupine Seabight," in *European margin dynamics. Side-scan sonar and seismic images*. Editors J. Mienert and P. Weaver (Berlin: Springer), 183–186. doi:10.1029/2003eo190009

White, M. (2007). Benthic dynamics at the carbonate mound regions of the Porcupine Sea Bight continental margin. *Int. J. Earth Sci.* 96, 1–9. doi:10.1007/s00531-006-0099-1

Zaragosi, S., Bourillet, J. F., Eynaud, F., Toucanne, S., Denhard, B., Van Toer, A., et al. (2006). The impact of the last European deglaciation on the deep-sea turbidite systems of the Celtic-Armorican margin (Bay of Biscay). *Geo-Marine Lett.* 26, 317–329. doi:10.1007/s00367-006-0048-9